ESD-TR-75-299

Technical Note

1975-25

Radiation Pattern Calculations for a Waveguide Lens Multiple-Beam Antenna Operating in the AJ Mode

B. M. Potts

14 October 1975

Prepared for the Defense Communications Agency
under Electronic Systems Division Contract F19628-76-C-0002 by

Lincoln Laboratory
MASSACHUSETTS INSTITUTE OF TECHNOLOGY
LEXINGTON, MASSACHUSETTS

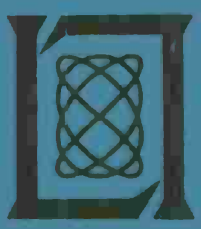

The work reported in this document was performed at Lincoln Laboratory, a center for research operated by Massachusetts Institute of Technology, for the Military Satellite Office of the Defense Communications Agency under Air Force Contract F19628-76-C-0002.

This technical report has been reviewed and is approved for publication.

FOR THE COMMANDER

Eugene C. Raabe

Eugene C. Raabe, Lt. Col., USAF
Chief, ESD Lincoln Laboratory Project Office

MASSACHUSETTS INSTITUTE OF TECHNOLOGY

LINCOLN LABORATORY

RADIATION PATTERN CALCULATIONS FOR A WAVEGUIDE LENS MULTIPLE-BEAM ANTENNA OPERATING IN THE AJ MODE

B. M. POTTS

Group 61

TECHNICAL NOTE 1975-25

14 OCTOBER 1975

LEXINGTON MASSACHUSETTS

ABSTRACT

The jammer suppression obtained with a multiple-beam antenna (MBA) by radiation pattern shaping is studied for applications with the DSCS III satellites. Results are presented for three separate MBA designs each consisting of an X-band waveguide lens excited by a multi-element feed cluster located in its focal plane. The first two designs are for a 28-inch diameter lens with 19- and 61-element clusters; the third MBA design is for a 50-inch lens using a 61-element feed cluster.

To demonstrate the AJ performance of each MBA, calculations were carried out for a large number of jammer locations distributed over the surface of the earth. At each location, the jammer suppression is achieved by adjusting the amplitude excitation of the feed elements to create an earth-coverage radiation pattern with a minimum located in the direction of the jammer. The methods used to achieve jammer protection are deliberately restricted to control of amplitude, plus the switching of phase between very restricted states, in order to assess the performance of a relatively simple, non-adaptive approach.

Results which characterize the AJ performance of each MBA in terms of the null level at the jammer, null coverage area and frequency dependence are presented.

CONTENTS

GLOSSARY

AJ	Anti-jam
DSCS	Defense satellite communication system
EC	Earth-coverage
ECPMIN	Earth-coverage with prescribed minima
FOV	Field of view (usually $\pm 9°$ to cover the earth from synchronous orbit)
MBA	Multiple-beam antenna
NS	Null steering
RNL	Relative null level

Radiation Pattern Calculations for a Waveguide Lens
Multiple-Beam Antenna Operating in the AJ Mode

I. Introduction

One of the intended uses of a multiple-beam antenna (MBA) in the receive mode on the DSCS III satellite is that of suppressing interfering sources, or jammers located on the surface of the earth, by radiation pattern shaping. A particularly useful radiation pattern shape for this purpose is one which provides uniform coverage of that portion of the earth's surface visible from the satellite with the exception of points where the interfering signals originate. In a previous note [1] some relatively simple methods for producing earth-coverage patterns with prescribed minima (ECPMIN) were discussed and contour plots illustrating the types of null* coverages which could be obtained within an 18 degree field-of-view (FOV) were presented.

The purpose of this memorandum is to study a 19-beam and 61-beam MBA with the aim of determining the extent to which a jammer may be suppressed as a function of frequency and as a function of its location on the surface of the earth. Three separate MBA designs were considered. The first two configurations are for a 28-inch diameter waveguide lens with 19- and 61-element feeds having feed element spacings of 2.35 and 1.30 inches, respectively. These dimensions correspond to the optimum values for optimizing the nulling performance over an 18 degree FOV [2]. The third MBA design is for a 61-

*In this report the term "null" will be used not to represent a complete zero in the antenna pattern, but in the colloquial sense of a relative minimum.

element feed using the same feed spacing as the 19-element feed (i.e., 2.35 inches), but with a lens diameter of 50 inches.

The following section presents the analytical approach used for calculating the AJ performance over the surface of the earth for a MBA system located in a geosynchronous orbit. This section is followed by calculations which illustrate the jammer suppression achieved with the 19- and 61-element feed systems. In the final section, radiation pattern calculations are presented which illustrate the nulling performance over the earth's surface for several selected jammer locations.

II. Methodology for Calculating the AJ Performance Over the Earth's Surface

Figure 1 illustrates the geometry which was used for calculating the AJ performance over the surface of the earth. The coordinates of the jammer location are specified in terms of the longitude coordinate, α, and latitude coordinate,* β, relative to the earth coordinate frame (x,y,z). The MBA is assumed to be located in a geosynchronous orbit with the antenna boresight axis (i.e., the lens axis) lying in the equatorial plane and intersecting the earth longitude coordinate at α_o. Given the location of the jammer (α,β) and the location of the satellite α_o, it can be shown that the (θ,ϕ) coordinates of the jammer relative to the antenna coordinate system (x',y',z') are given by

$$\theta = \tan^{-1}\left[\frac{\sqrt{\sin^2(\beta) + \cos^2(\beta) \cdot \sin^2(\alpha-\alpha_o)}}{k - \cos(\beta) \cdot \cos(\alpha-\alpha_o)}\right] \tag{1}$$

$$\phi = \begin{cases} \tan^{-1}[\cos(\beta) \cdot \sin(\alpha-\alpha_o)], & \beta \neq 0 \\ \pi/2, & \beta = 0,\ \alpha > \alpha_o \\ -\pi/2, & \beta = 0,\ \alpha < \alpha_o \\ 0, & \beta = \alpha = 0 \end{cases} \tag{2}$$

where

$$k = \frac{\text{orbit altitude relative to (x,y,z) origin}}{\text{mean radius of the earth}}$$

*All latitudes are measured $\pm 90°$ with latitudes North taken as positive and all longitudes are measured $\pm 180°$ with respect to the prime meridian (Greenwich, Eng.) with longitudes East taken as positive.

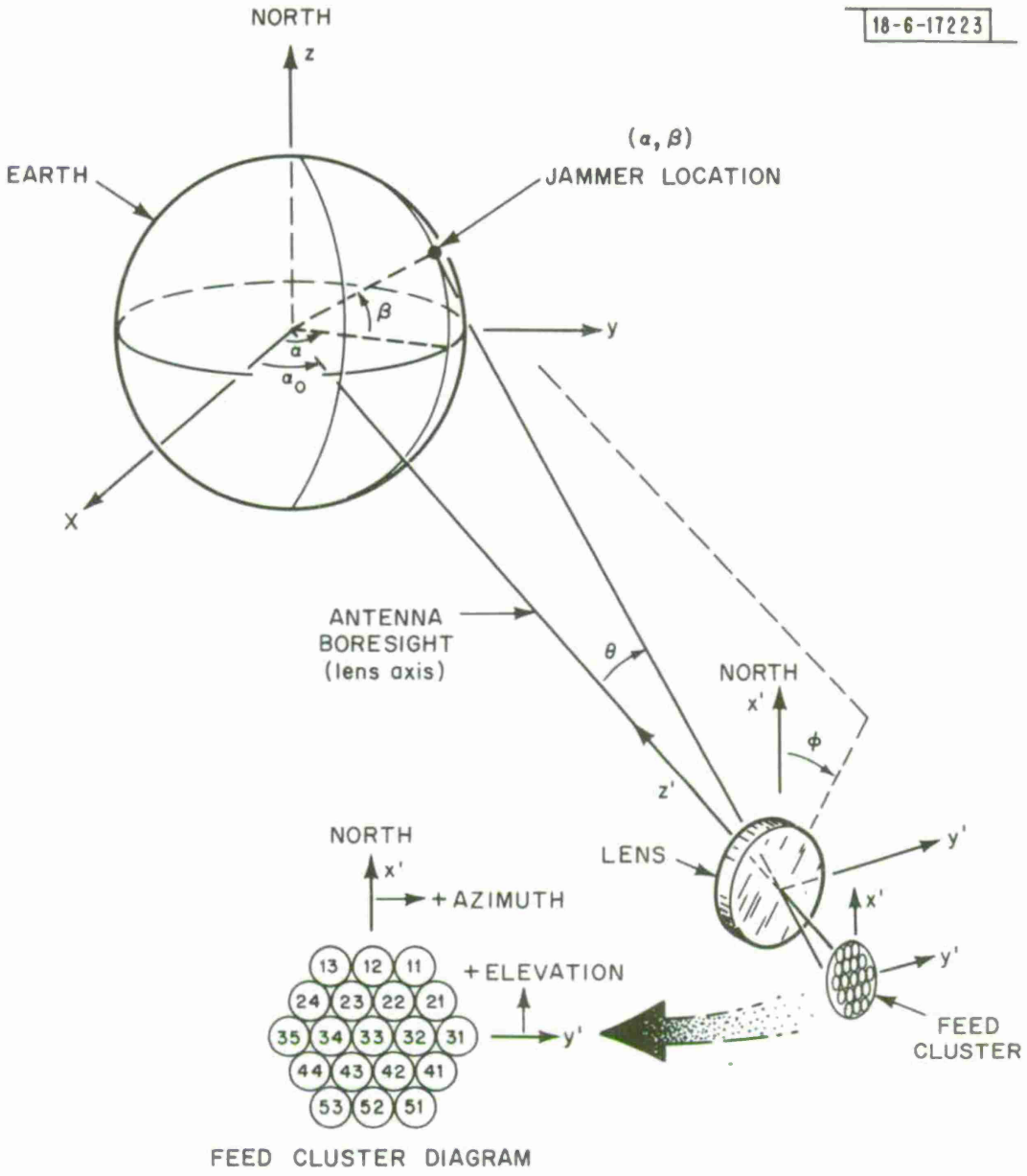

Fig. 1. Earth-satellite geometry for calculating the AJ performance over the surface of the earth.

$$k \simeq \frac{22,300 + 3959}{3959} = 6.6327$$

One can also specify the location of the jammer in the antenna coordinate system in terms of the elevation and azimuth coordinates (el and az, respectively) using Fig. 2 and the transformation equations

$$el = \tan^{-1}[\tan(\theta) \cdot \cos(\phi)] \tag{3}$$

$$az = \tan^{-1}[\tan(\theta) \cdot \sin(\phi)] \tag{4}$$

Thus from Eqs. (1)-(4) it is possible to calculate the direction (θ,ϕ or el, az) in which a null must be produced in an earth-coverage pattern in order to suppress a jammer located on the surface of the earth at the coordinates α,β.

To evaluate the AJ performance, one must first determine all possible ways in which a null can be produced at the jammer location. For the feed cluster shown in Fig. 1 with the feed elements arranged on a triangular grid, this requires considering one-sixth of the total aperture since the cluster is periodic with six-fold symmetry.* Figure 3 illustrates one way in which a 19-element feed cluster can be subdivided into six equal parts, with the x' and y' axes representing the N-S and E-W directions, respectively. If one were to consider, for example, only section 4 of the feed cluster then by selectively turning off the feeds in this section, nulls would be produced at those points on the earth's surface lying in section 1, that is, for $|\phi| \leq 30°$. If the desired null direction lies outside of section 1 (i.e., $|\phi| > 30°$), one would simply transform that point so that it lies within sector 1 using the trans-

*To be exact, it would be necessary to consider one-fourth of the feed cluster since the waveguide lens is four-fold symmetric. However, the error introduced into the calculations by considering only one-sixth of the feed cluster has been found to be negligible.

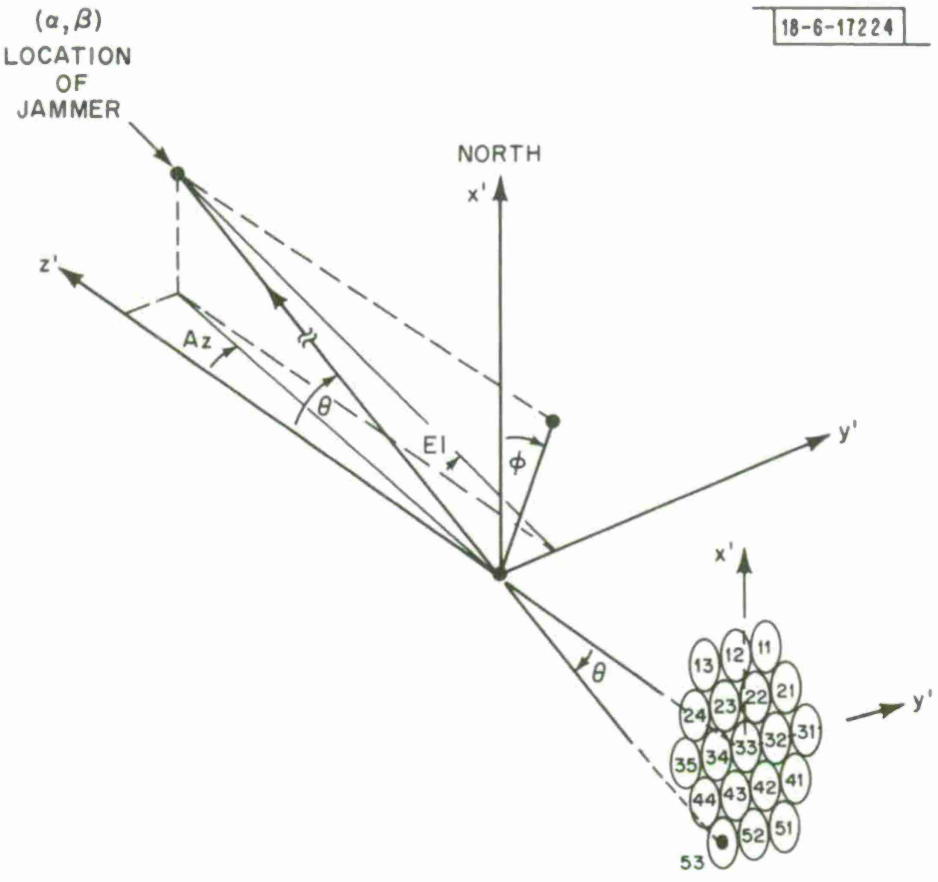

Fig. 2. Relationship between earth coordinates (α,β) of the jammer location and the antenna coordinates (θ,ϕ) and (Az, El).

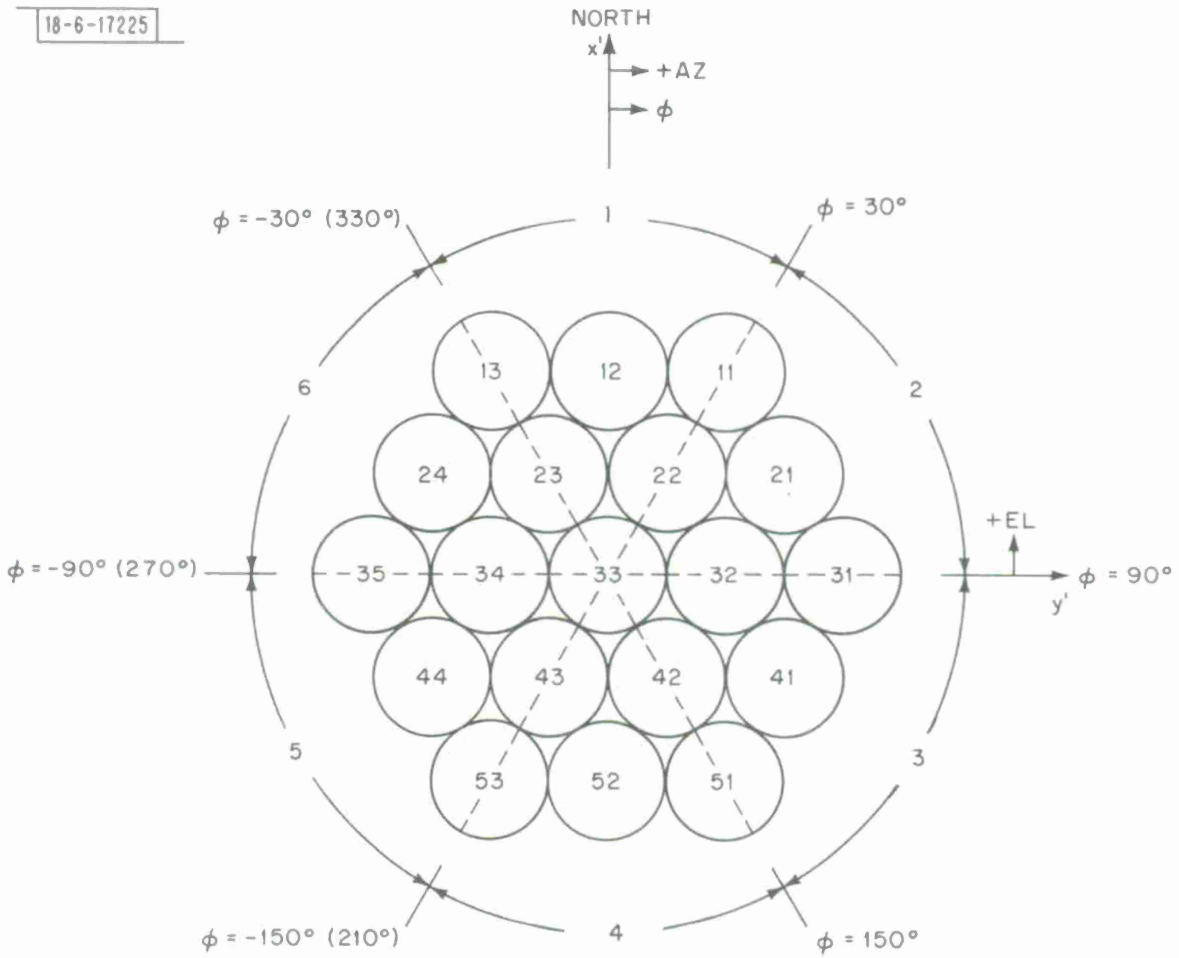

Fig. 3. 19-Element feed cluster subdivided into six equal parts.

formation,

$$\phi' = \phi - 60(\text{ISECT}-1) \tag{5}$$

where ϕ is the coordinate of the desired null direction, ϕ' the coordinate of the null direction relative to feed cluster section 1, and ISECT the feed cluster section associated with the original jammer location. Hence by using Eq. (5) it is possible to evaluate the AJ performance at any point on the earth's surface by considering only the nulls produced by the feed elements located in section 1 of the feed cluster.

To calculate an earth-coverage radiation pattern with prescribed minima (ECPMIN) all feed elements are excited except those which produce beams pointing closest to the direction of the interfering source or sources. For the 19-element feed cluster in Fig. 3 there are six ways in which a null can be produced in an earth-coverage pattern by turning off a single feed located in one section of the feed cluster. Certainly not all of these cases will produce a null at a given jammer location, however, for a jammer arbitrarily located in section 1 (or for an unknown jammer located in section 1) no more than six cases need be considered. When the jammer falls between two or three adjacent beams it is necessary to turn off those two or three beams to produce the required discrimination. For the 19-element feed cluster there are nine possible ways in which two adjacent feeds may be turned off and four ways in which a cluster of three beams may be turned off over one section of the feed cluster. Another method of producing nulls in an earth-coverage pattern is referred to as null steering (cf. Ref. 1) and consists of exciting all except two adjacent feed horns with in-phase and equal amplitude signals, say

0° and 1 volt, respectively. The remaining two adjacent feed horns are excited with -90° and 90° relative phase. By varying their relative amplitudes between 0 and $\sqrt{2}$ volts, the minimum in the radiation pattern can be made to move or "steer" as a function of the amplitude ratio. By including null steering as a method for producing nulls in an earth-coverage pattern there are an additional 9n possibilities, where n is equal to the number of increments used in dividing the power between the two adjacent quadrature phase excited feeds. Thus if one considers the 19-beam system for producing nulls on the earth's surface by either turning off a single feed, two adjacent feeds, three adjacent feeds or null steering (with n = 5), there are a total of 65 cases* which must be considered at each jammer location.

For the 61-beam system there are approximately three times as many feed elements as in the 19-beam system; consequently, the combined area occupied by any three feed elements is approximately equal to the area of a single feed element for the 19-beam system provided that both feed clusters are designed for the same lens diameter. It follows that the null coverage area obtained from the 61-element feed cluster by turning off three feed elements is approximately the same as the null coverage area for the 19-beam system obtained by turning off a single feed. Therefore, rather than turn off a single feed to produce a null as was done with the 19-beam system, one would turn off a cluster of three feeds for the 61-element feed system. Since there are 15 feed elements located in any one section of the feed cluster (see Fig. 4),

*Also included is the special case where the center feed 33 is partially turned on but excited 180° out of phase with the remaining feed elements so as to create a null near the sub-satellite point (i.e., az ≃ 0°, el ≃ 0°).

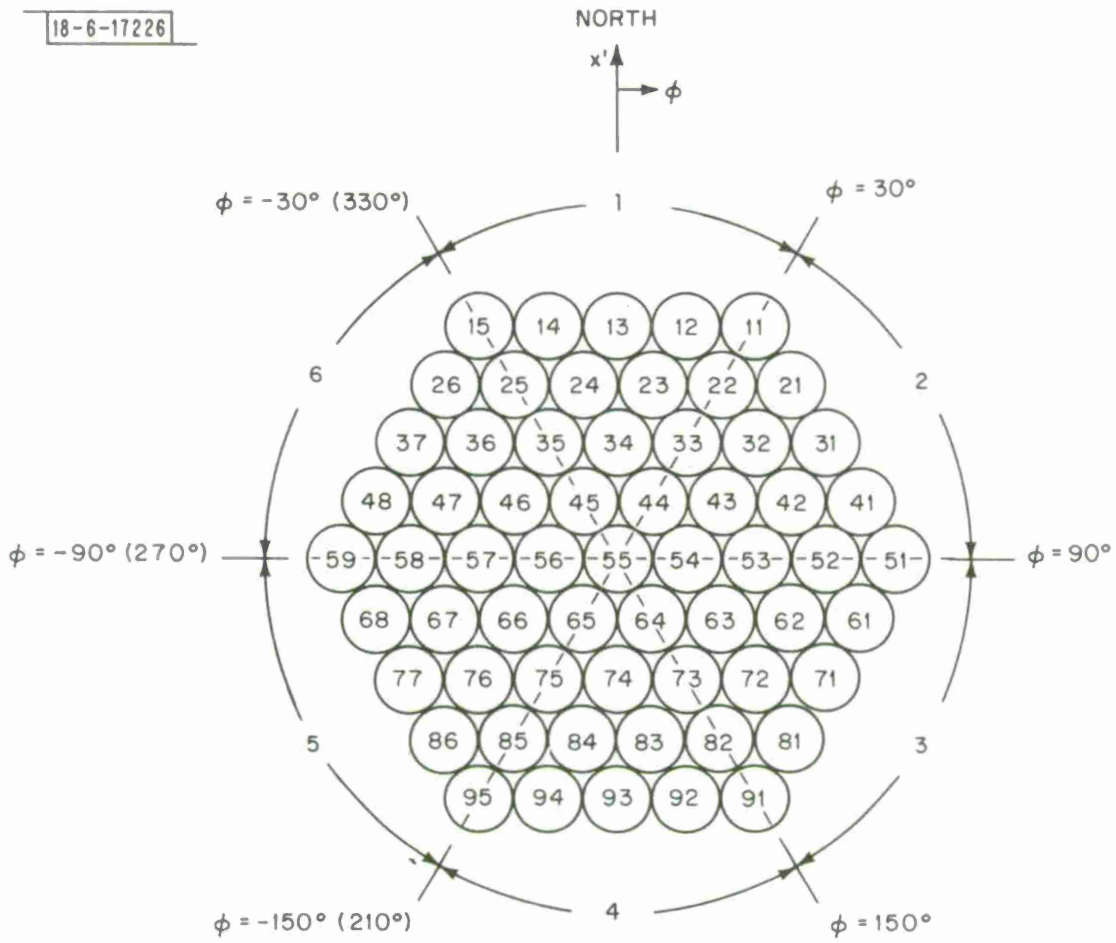

Fig. 4. 61-Element feed cluster subdivided into six equal parts.

there are a total of 16 ways in which a cluster of three feeds may be turned off. This compares with the six ways in which nulls may be produced by turning off a single beam in the 19-beam system. As a result, the null coverage areas obtained by turning off clusters of three feeds is such that, for a given null level, the coverage areas overlap much more than in the 19-beam system. Furthermore, if the three feeds used in producing the null are turned on by an appropriate amount and excited 180° out-of-phase with the remaining feeds the null coverage area is further enhanced.

One of the disadvantages of the 28-inch diameter lens is the fact that the null coverage areas produced on the surface of the earth are generally much larger than required for suppressing a single jammer. To reduce the null coverage area while at the same time maintaining the same FOV, requires using a larger lens and more feed elements. In order to study this case, calculations were also carried out for a 61-element feed using the same feed spacing as the 19-element feed, but with a lens diameter of 50 inches. Two methods of producing nulls in an earth-coverage pattern were considered for the 50-inch lens; these were null steering and single beam suppression. Since there are a total of 15 ways of turning off a single feed and 30 ways of turning off two adjacent feeds over one section of the 61-element feed, there exists a total of 165 ways in which a null can be produced by either turning off a single feed or null steering (with n = 5).

The procedure for determining the AJ performance of the MBA consisted simply of calculating the null level (i.e., the ECPMIN pattern) at a large number of points over the surface of the earth. At each point all possible

ways of producing a null are considered; for the 28-inch diameter lens this requires evaluating the 65 possibilities of producing a null for the 19-feed system and 17* possibilities for the 61-element feed system. For the 50-inch lens system, a total of 165 cases must be considered at each point. Although it might appear that computing all of the ECPMIN patterns would be time consuming, the total amount of computation required is considerably less than one might expect. The 19-beam system, for example, requires only that the EC pattern and the single beam patterns for each of the six feeds located in one section of the feed cluster be calculated at each sample point on the earth's surface. With this information all 65 cases can be obtained simply by subtracting the complex field patterns of the appropriate single beam patterns (with the proper weighting factors) from the complex EC pattern.

Figure 5 illustrates how the jammer locations are distributed over the earth's surface. A total of 1147 sample points† are considered by varying the longitude and latitude coordinates over the range $0° \leq \alpha \leq 90°$ and $0° \leq \beta \leq 75°$ in increments of 2.5°. For each sample point there is associated an increment of surface area, A_{ij}, given by

---

*Also included as a special case for the 61-beam system is the case where the center feed 55 is excited partially but 180° out of phase with the remaining feeds so as to produce a null near the sub-satellite point.

†For the 50-inch diameter lens a total of 1073 sample points were considered over the range $0° \leq \alpha \leq 90°$, $0° \leq \beta \leq 70°$ in increments of 2.5°.

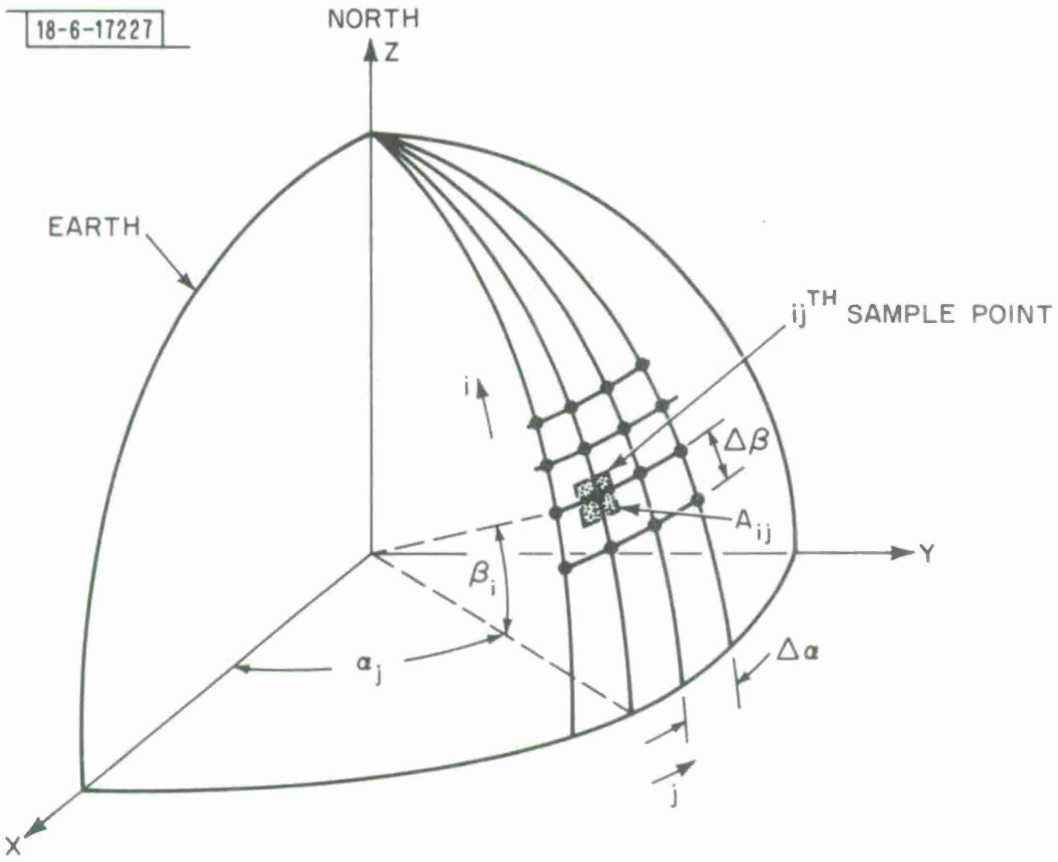

Fig. 5. Diagram illustrating the distribution of jammer locations over the surface of the earth.

$$A_{ij} = \int_{\alpha_j-1/2\Delta\alpha}^{\alpha_j+1/2\Delta\alpha} d\alpha \int_{\beta_i-1/2\Delta\beta}^{\beta_i+1/2\Delta\beta} \cos(\beta)d\beta, \qquad \begin{matrix} i = 1,2,\cdots,N \\ j = 1,2,\cdots,M \end{matrix} \tag{5}$$

which can be approximated as

$$A_{ij} = \Delta\alpha_j \cdot \begin{cases} \sin(1/2\Delta\beta) & , i = 1 \\ \sin(\beta_i+1/2\Delta\beta)-\sin(\beta_i-1/2\Delta\beta) & , i = 2,\cdots,N-1 \\ \sin(\beta_m) - \sin(\beta_m-1/2\Delta\beta) & , i = N \end{cases} \tag{6}$$

where

$$\Delta\alpha_j = \begin{cases} 1/2\ \Delta\alpha = \alpha_m/2(M-1) & , j = 1,M \\ \Delta\alpha = \alpha_m/(M-1) & , \text{otherwise} \end{cases}$$

$$\Delta\beta = \frac{\beta_m}{N-1}$$

$$\beta_i = \frac{i-1}{N-1}\ \beta_m$$

α_m = maximum value of α

β_m = maximum value of β

N = number of sample points in latitude

M = number of sample points in longitude

The incremental area A_{ij} is defined to be the area over which the null level, evaluated at the ij^{th} sample point, exists. Thus the total surface area

occupied by a particular null level is obtained by summing the values of A_{ij} at each sample point for which the desired null level is achieved. By quantizing the null levels in one dB increments, say from 0 dB to -50 dB,* the total surface area occupied by each null level is given by

$$A_k = \sum_{j=1}^{M} \sum_{i=1}^{N} (\varepsilon_k)_{ij} A_{ij}, \quad k=1,2,\cdots,51 \tag{7}$$

where

A_1 = total surface area occupied by null levels from 0 to -1 dB

A_2 = total surface area occupied by null levels from -1 to -2 dB

. . .

A_{50} = total surface area occupied by null levels from -49 to -50 dB

A_{51} = total surface area occupied by null levels less than -50 dB

and

$$(\varepsilon_k)_{ij} = \begin{cases} 1 & -k \text{ db} < \text{Null level at } ij \leq -k+1 \\ 0 & \text{otherwise} \end{cases}$$

Using Eq. (7), the total surface area within the range $0 \leq \alpha \leq \alpha_m$, $0 \leq \beta \leq \beta_m$ can be calculated as

*Null levels are specified relative to the peak directive gain of the EC pattern.

$$A_T = \sum_{k=1}^{51} A_k \tag{8}$$

and, hence, from (7) and (8) the percentage of the total area occupied by each null level is given by

$$\eta_k = \frac{100A_k}{A_T}, \qquad k = 1,2,\cdots,51 \quad . \tag{9}$$

III. Null Level Calculations

The results presented in this section illustrate the jammer suppression which can be achieved with the 19- and 61-element feed systems. Three separate MBA designs are considered. The first two are for a 19- and 61-element feed system using a 28-inch diameter lens. This lens diameter corresponds to the optimum diameter for optimizing the null level over an 18° FOV when feed element spacings of 2.35 and 1.30 inches are used for the 19- and 61-element feed clusters, respectively. The lens center design frequency was chosen to be 8.15 GHz which represents the center of the receive band of the DSCS III satellite. The third MBA design is a 61-element feed system using the same feed spacing as the 19-element feed (i.e., 2.35 inches) but with a lens diameter of 50 inches.

The analysis assumes that the feed horns are circularly polarized with the feed elements arranged on a planar hexagonal lattice as indicated in Fig. 1. The directive gain of a single feed horn is adjusted so that its element gain corresponds to the gain which would be obtained if the entire hexagonal area between the feed elements were uniformly illuminated. The amplitude excitation of the feed horns is assumed to be the same with the exception of six feeds in the outer ring which are excited slightly more than the remaining feeds so as to improve the EC pattern by making it conform more closely to the desired circular FOV. For the 19-element cluster, feeds 12, 21, 24, 41, 44 and 52 are excited .83 dB more than for the remaining feeds. For the 61-element clusters, feeds 13, 31, 37, 71, 77 and 93 are excited 1.59 dB more than the remaining feeds for the 28-inch lens and .34 dB more than the

remaining feeds for the 50-inch lens. The phase distribution across the feed clusters is also adjusted so as to compensate for the unequal path length from each feed element to the vertex of the lens.

A. 19-Element Feed with 28-Inch Diameter Lens

The DSCS III receive MBA is designed to operate over an approximate bandwidth of 350 MHz from 7.975 to 8.325 GHz. Figure 6 presents a diagram showing the jammer suppression (i.e., the minimum null level) which can be achieved with the 19-beam system over this frequency range, plotted as a function of the percentage of the earth's surface coverage area. The data in this figure is calculated by considering a total of 1147 jammer locations on the earth between $0° \leq \alpha \leq 90°$ and $0° \leq \beta \leq 75°$ for $\Delta\alpha = \Delta\beta = 2.5°$. The null level at each jammer location is determined by first calculating the 65 ECPMIN patterns at the center frequency of the lens, that is, at f = 8.15 GHz. From these 65 patterns the "optimum" null level is represented by the ECPMIN pattern which produces the lowest directive gain. This ECPMIN pattern is then recomputed at the edge frequencies (i.e., 7.975 and 8.325 GHz) to determine the jammer suppression at these frequencies. The null levels obtained at the jammer locations are calculated* in terms of the absolute directive gain (in dBi), however, for convenience in presenting the data the null levels in Fig. 6 are plotted on a relative scale such that 0 dB corresponds to the peak directive gain of the earth-coverage pattern.

*For a discussion of the computer program used for calculating the ECPMIN patterns see Appendix A, Reference 2.

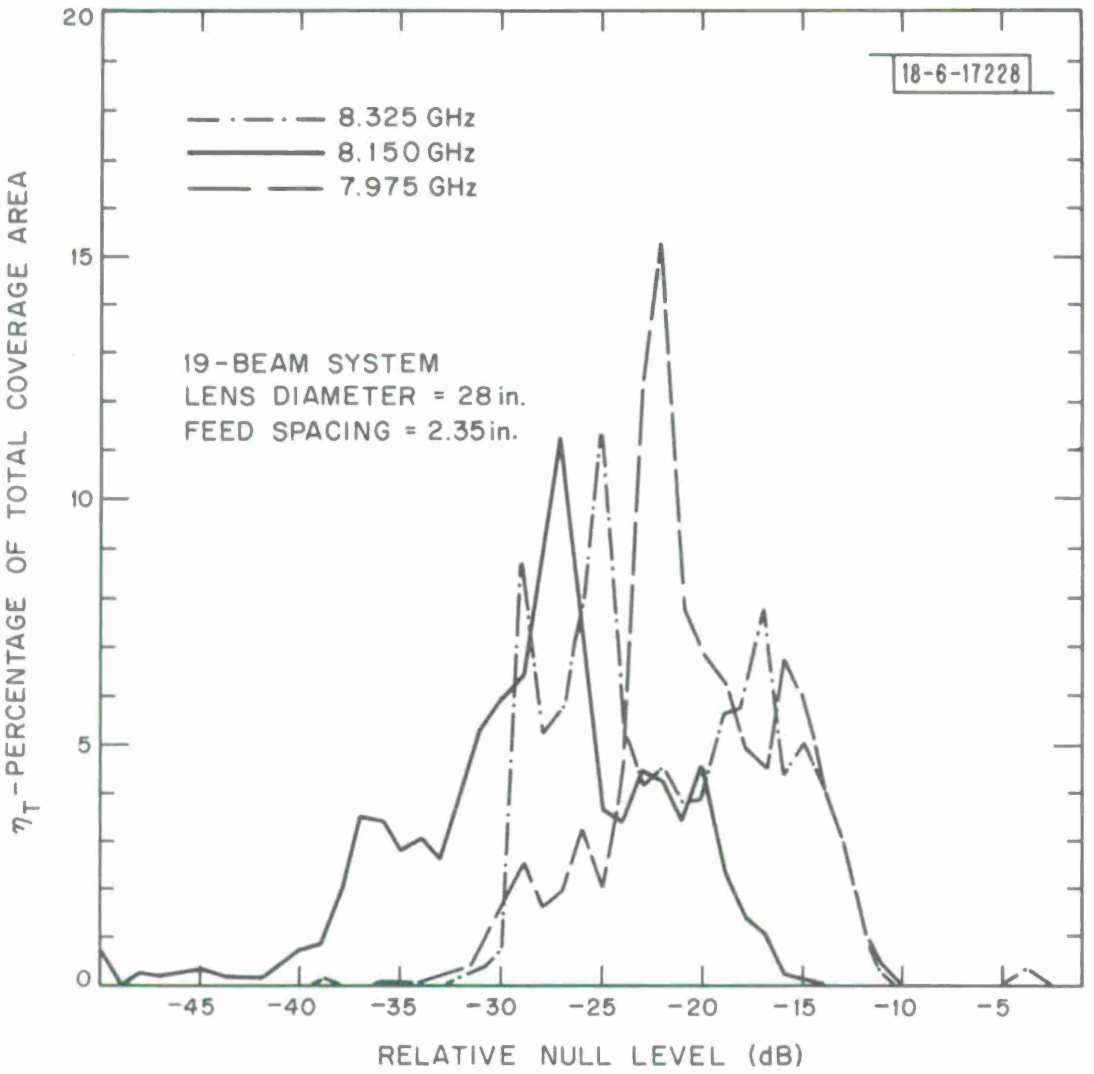

Fig. 6. Nulling performance for the 19-element feed cluster obtained by turning off a single feed, two adjacent feeds, three adjacent feeds and null steering.

It is interesting to note that of the 1147 jammer locations approximately 93 percent of these were suppressed by turning off either two or three beams whereas only 7 percent were suppressed by turning off a single feed or null steering. This is largely the result of the fact that the criterion for judging the null performance is based on achieving the lowest directive gain at the jammer location, and it merely indicates that lower null levels can be achieved by turning off two or three beams. However, since considerably larger null coverage areas can be expected when two or three beams are turned off, these results indicate a very high probability of having the communications link degraded to any user located in the general vicinity of the jammer. Consequently it appears worthwhile to also consider the nulling performance obtained when the ECPMIN patterns are calculated on the basis of only turning off a single beam or null steering. Since both of these methods for producing nulls create essentially the same null coverage area, one would expect that the null coverage area would be considerably reduced below that obtained with two or three beams off. Figure 7 illustrates the results of the ECPMIN calculations obtained on the basis of either turning off a single beam of null steering. Comparing this figure with Fig. 6, it is observed that the median null level in Fig. 7 is degraded by approximately 6 or 7 dB. As shown in Table I, the median null level increases from approximately -28 dB to -21 dB at the center frequency and from approximately -23 dB to -17 dB at the edge frequencies.

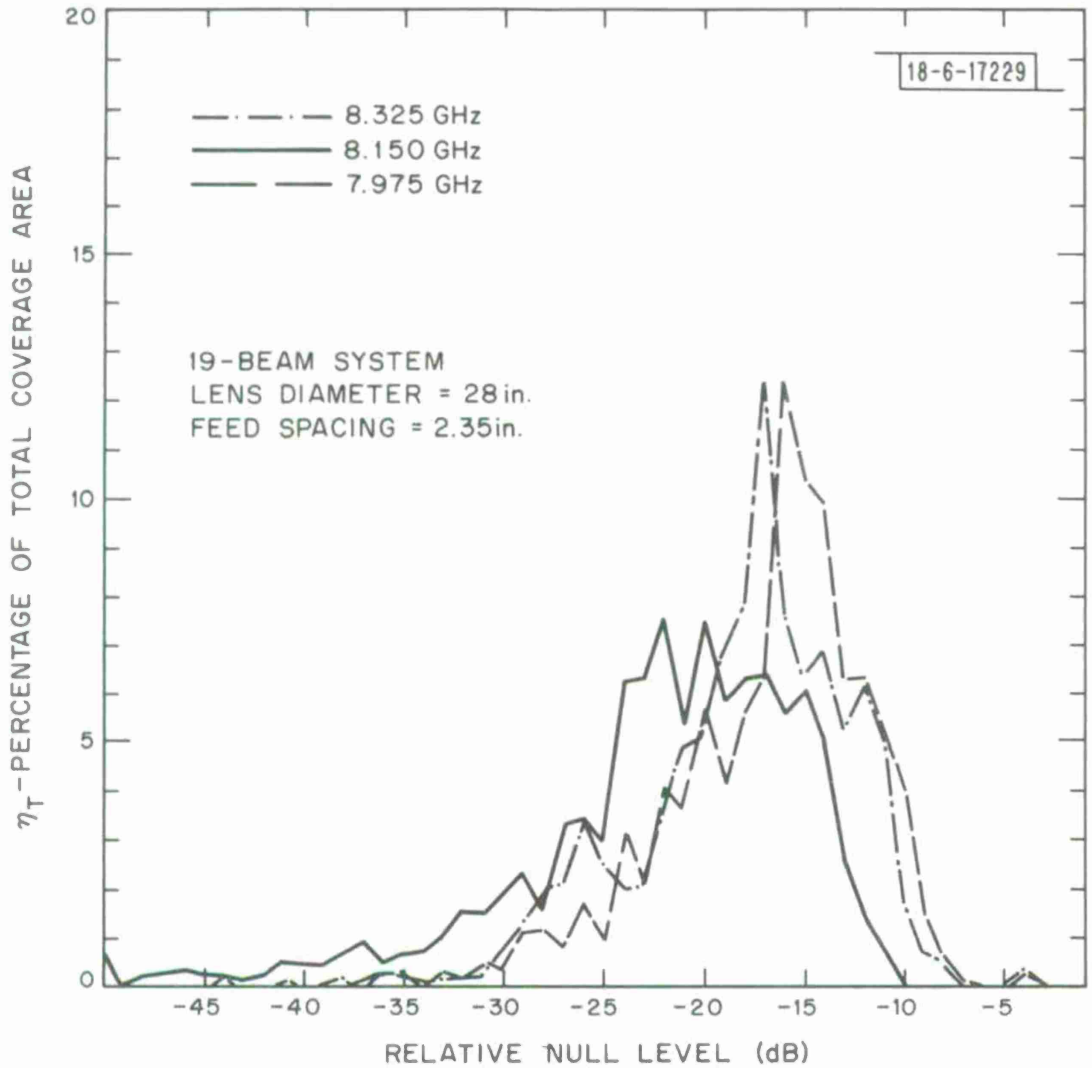

Fig. 7. Nulling performance for the 19-element feed cluster obtained by turning off a single feed and null steering.

TABLE I

Comparison of ECPMIN Calculations

Frequency (GHz)	Median Null Level (dB)	
8.150	-28	ECPMIN Patterns Calculated with: (a) Single Beam Off, (b) Two Adjacent Beams Off, (c) Three beams off and (d) Null Steering
8.325	-23	
7.975	-22	
8.150	-21	ECPMIN Pattern Calculated with: (a) Single Beam Off and (b) Null Steering.
8.325	-18	
7.975	-16	

Figures 6 and 7 illustrate the nulling effectiveness in dB plotted in terms of the coverage area on the earth. Hence, for a given null level one can easily determine the percentage of the total earth's surface area within the coverage area which can be covered by that particular null level. It therefore follows that the total area under the curves between any two null levels represents the percentage of the total coverage area which can be covered by these null levels. Figure 8 is obtained by summing the areas under the curves in Figs. 6 and 7 and plotting the result (i.e., the percentage of the total coverage area) as a function of the null level. The thin-lined curves in Fig. 8 represent the results obtained from Fig. 6 when all 65 ECPMIN patterns are considered. These curves show, for example, that at the center frequency (8.15 GHz) the entire coverage area can be covered by a null level of -15 dB, and that approximately 94 percent of the coverage area can be covered by a null level of -20 dB. At the edge frequencies, the nulling performance is degraded due to the dispersive properties of the waveguide lens and for the -15 dB and -20 dB null levels the coverage drops to approxi-

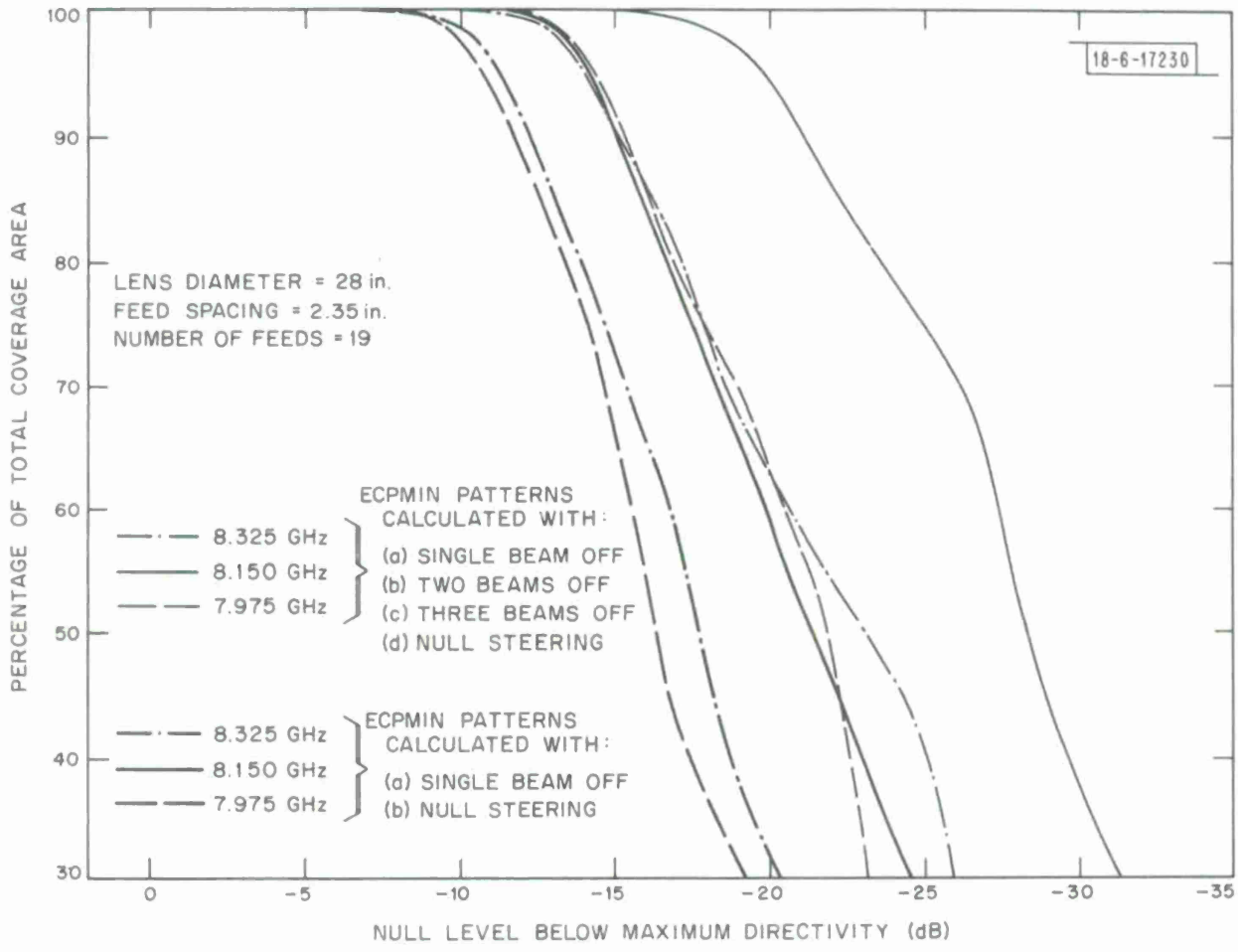

Fig. 8. Surface coverage area (in percent) vs. maximum null level for a 28-inch/19-feed MBA.

mately 91.5 and 63 percent, respectively.

The thick-lined curves in Fig. 8 represent the performance obtained when the ECPMIN pattern calculations are based on turning off a single feed and null steering. As mentioned earlier, for these cases the null level performance is degraded as evident by the fact that the curves are shifted to the left (i.e., in the direction of decreasing null levels) by several dB. The null performance at the center frequency (8.15 GHz) corresponds to approximately the same level of performance as obtained at the edge frequencies when all 65 ECPMIN patterns are considered.

Figures 9 and 10 are contour plots showing the null coverage performance over the earth's surface plotted as a function of the earth longitude and latitude coordinates for null levels ranging from -10 to -20 dB (clear), -20 to -30 dB (cross hatched), -30 to -40 dB (shaded) and less than -40 dB (dotted). These contours are plotted to illustrate the nulling levels which can be achieved over the earth's surface when the boresight axis of the MBA is centered at $\alpha = \alpha_o = 0°$. Figure 9 is obtained by considering all 65 ECPMIN patterns, whereas Fig. 10 is calculated by considering only nulls produced by either turning off a single feed or null steering. The deeper nulls obtained in Fig. 9 are indicated by the smaller portion of clear area (i.e., -10 to -20 dB null levels) and the larger amount of shaded area (-30 to -40 dB null levels). A comparison of Figs. 9 and 10 is indicated more concisely in Table II by tabulating the relative null level (RNL) as a function of the earth surface coverage area.

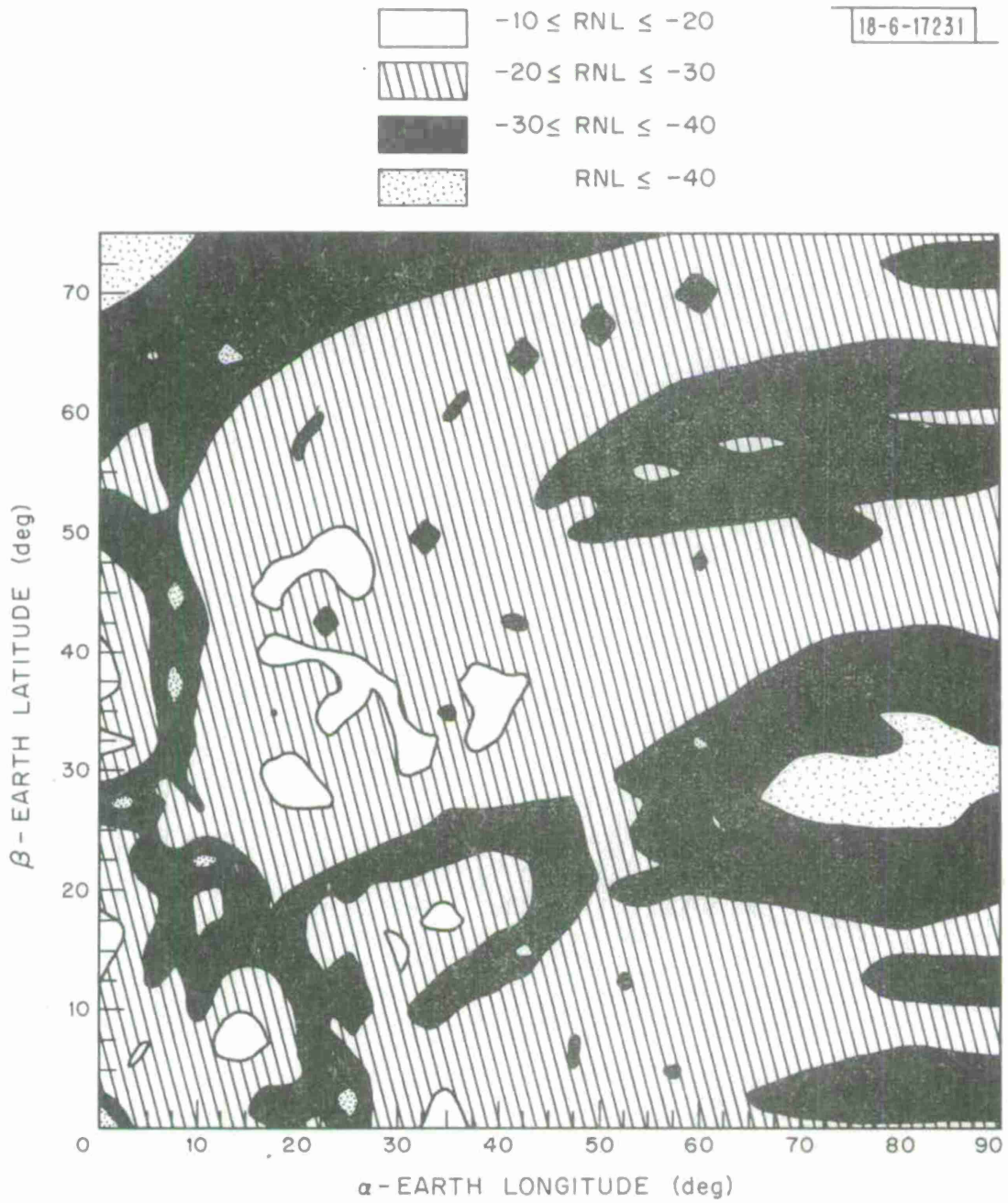

Fig. 9. Radiation pattern contour plot illustrating the null performance f = 8.15 GHz calculated on the basis of turning off a single feed, two adjacent feeds, three adjacent feeds and null steering.

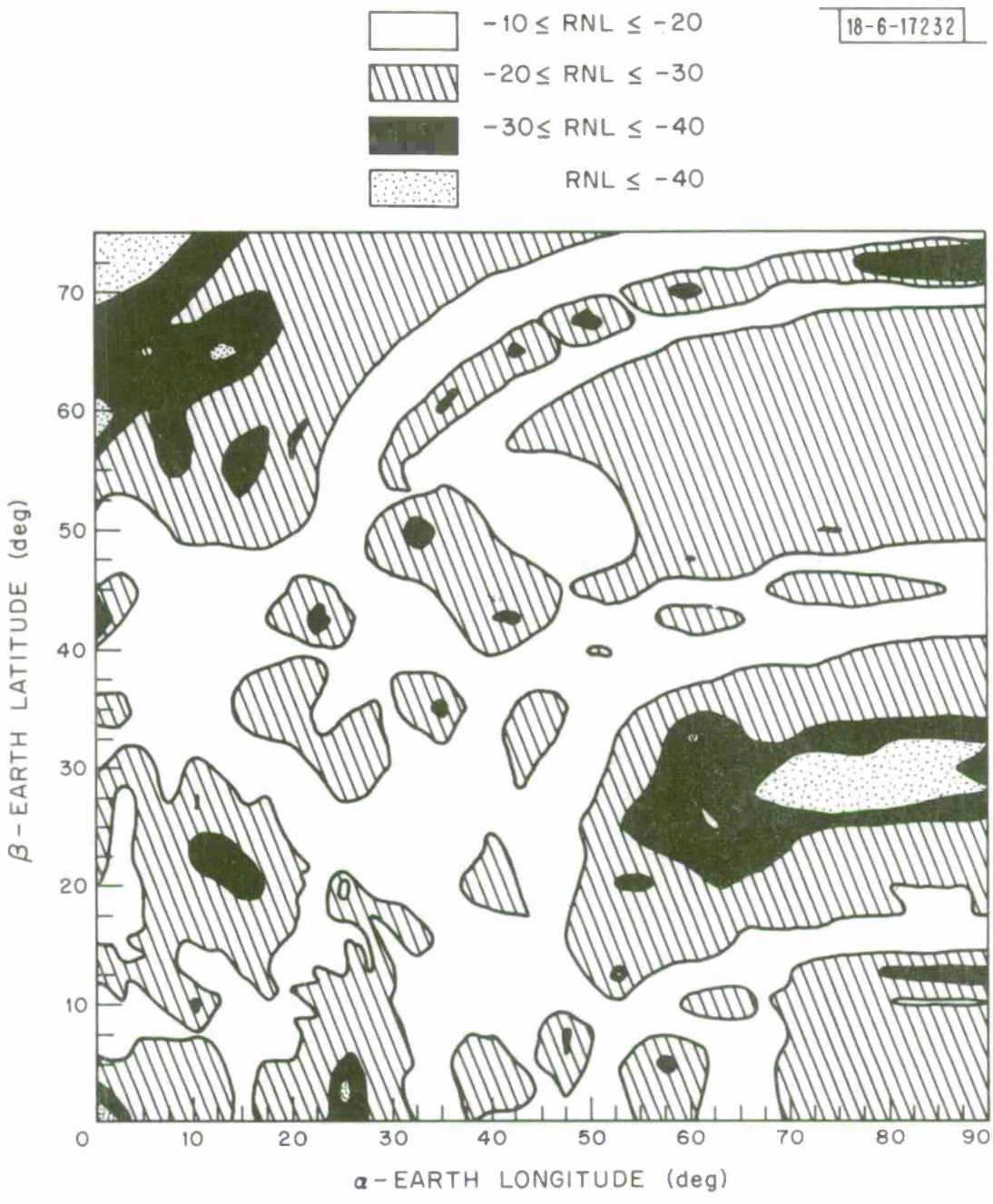

Fig. 10. Radiation pattern contour plot illustrating the null performance at f = 8.15 GHz, calculated on the basis of turning cff a single feed and null steering.

TABLE II

Relative Null Level (RNL) vs. Earth-Coverage Area

RNL (dB)	Earth-Coverage Area at 8.15 GHz (percent)	
	Fig. 10	Fig. 9
$-10 \leq$ RNL	0	0
$-20 \leq$ RNL < -10	47.62	9.92
$-30 \leq$ RNL < -20	41.31	58.54
$-40 \leq$ RNL < -30	8.43	28.46
RNL < -40	2.64	3.08
TOTAL	100.00	100.00

B. 61-Element Feed with 28-Inch Diameter Lens

In this section the results for the 61-element feed system are calculated using the same lens diameter and over the same frequency range as the 19-beam system. As mentioned earlier, the basic difference between these two systems is the fact that the 61-element feed cluster produces nulls by exciting all but three feeds. The three feeds used in producing the minima are partially turned on but excited 180° out-of-phase with the remaining 58 feeds. The amplitude weighting factors for the three feeds are determined in such a manner as to optimize the null level at the center frequency of the lens. These same weighting factors are used at the edge frequencies (i.e., 7.975 and 8.325 GHz) to calculate the null coverage behavior at these frequencies.

Figure 11 illustrates the nulling performance of the 61-element feed when plotted as a function of the percentage of the total earth's surface area within the coverage area. As in Fig. 6, the results of Fig. 11 are based on the statistics obtained from 1147 jammer locations on the earth's surface between $0° \leq \alpha \leq 90°$ and $0° \leq \beta \leq 75°$. The results in Fig. 11 clearly illustrate the frequency sensitivity of the null level when using a waveguide lens. At the

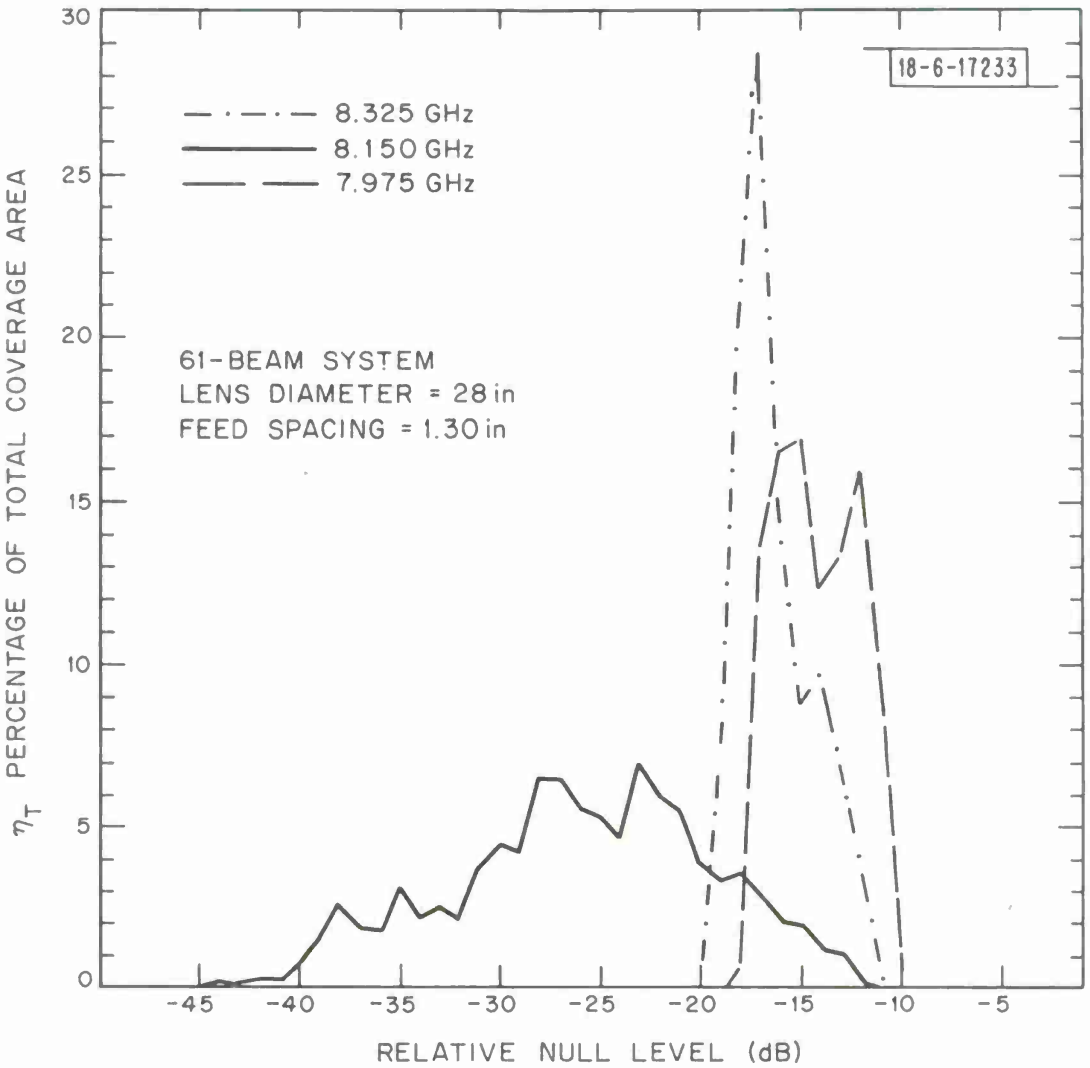

Fig. 11. Nulling performance for the 61-element feed and 28-inch diameter waveguide lens.

center frequency of the lens the null levels extend over a range of approximately 35 dB from -45 dB to -12 dB with a median level of -26 dB. Changing the frequency $\pm$175 MHz from the design frequency has the effect of reducing the range over which the null levels exist to about 10 dB (from $\simeq$ -20 dB to $\simeq$ -10 dB) and increasing the median null level from -26 dB at 8.15 GHz to -17 dB at 8.325 GHz and -15 dB at 7.975 GHz.

In order to verify that the deterioration in null level performance as a function of frequency is actually due to the dispersive properties of the waveguide lens, null level calculations were also carried out for a nondispersive lens. For calculation purposes a nondispersive lens is simulated using a waveguide lens but redesigning the lens at each frequency. The results of these calculations are shown in Fig. 12 and clearly illustrate the improvement which can be obtained for a nondispersive lens. For all three frequencies the median level varies by no more than 4 dB and lies between -27 dB and -23 dB.

Figure 13 through 15 are radiation pattern contour plots for the 61-element feed system which show the nulling performance of the waveguide lens. The effect of the frequency changes on the null level is clearly apparent by comparing the contour plot at the center frequency (Fig. 13) with the contour plots at f = 8.325 (Fig. 14) and f = 7.975 (Fig. 15).

The nulling effectiveness is illustrated more clearly in Fig. 16 by summing the areas under the curves in Figs. 11 and 12 and plotting the result as a function of the null level in dB. The results in this figure are equivalent to those shown in Fig. 8 for the 19-beam system. These two figures illustrate, for example, that at the center frequency and for a given surface coverage

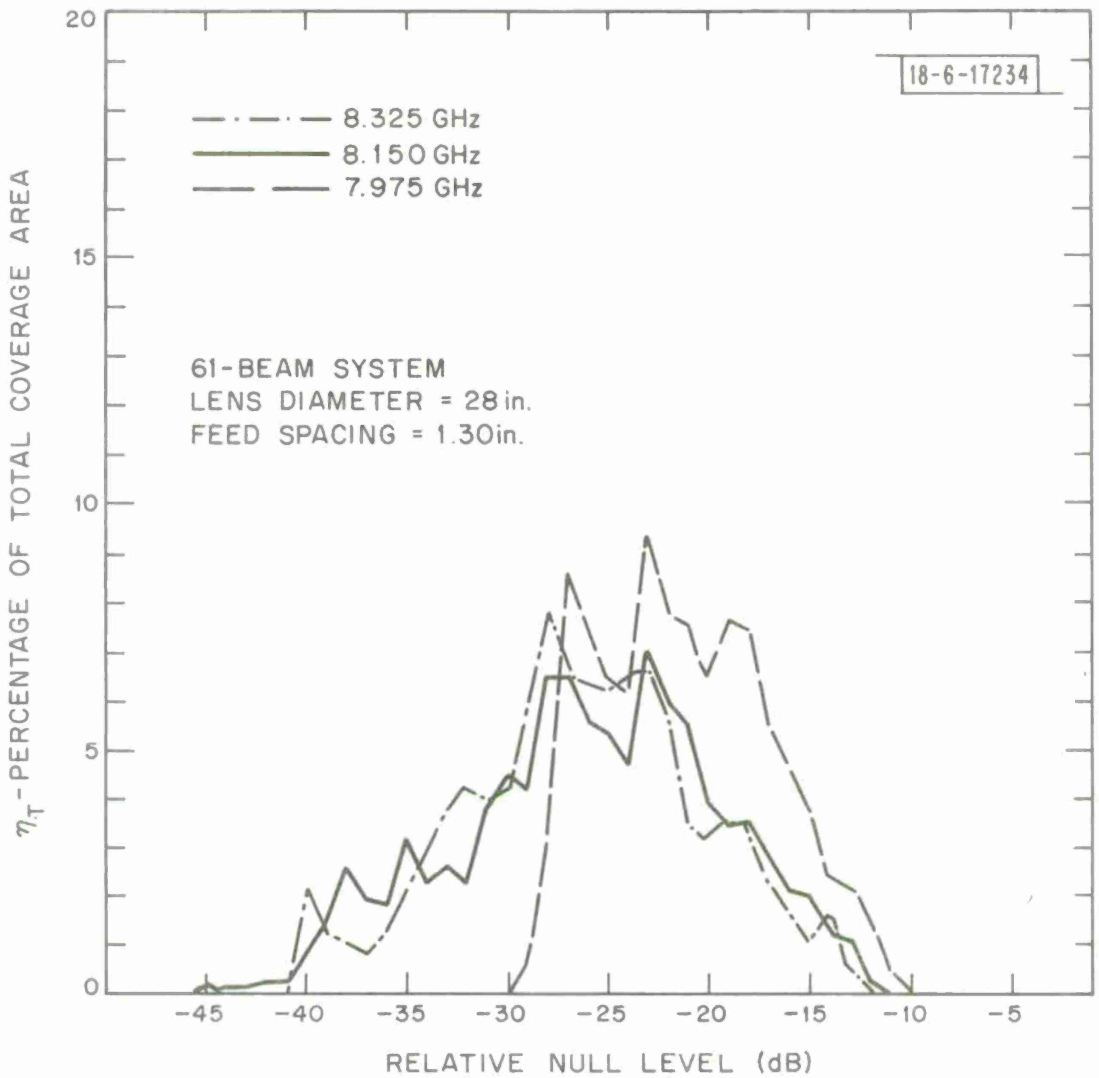

Fig. 12. Nulling performance for the 61-element feed and 28-inch nondispersive lens.

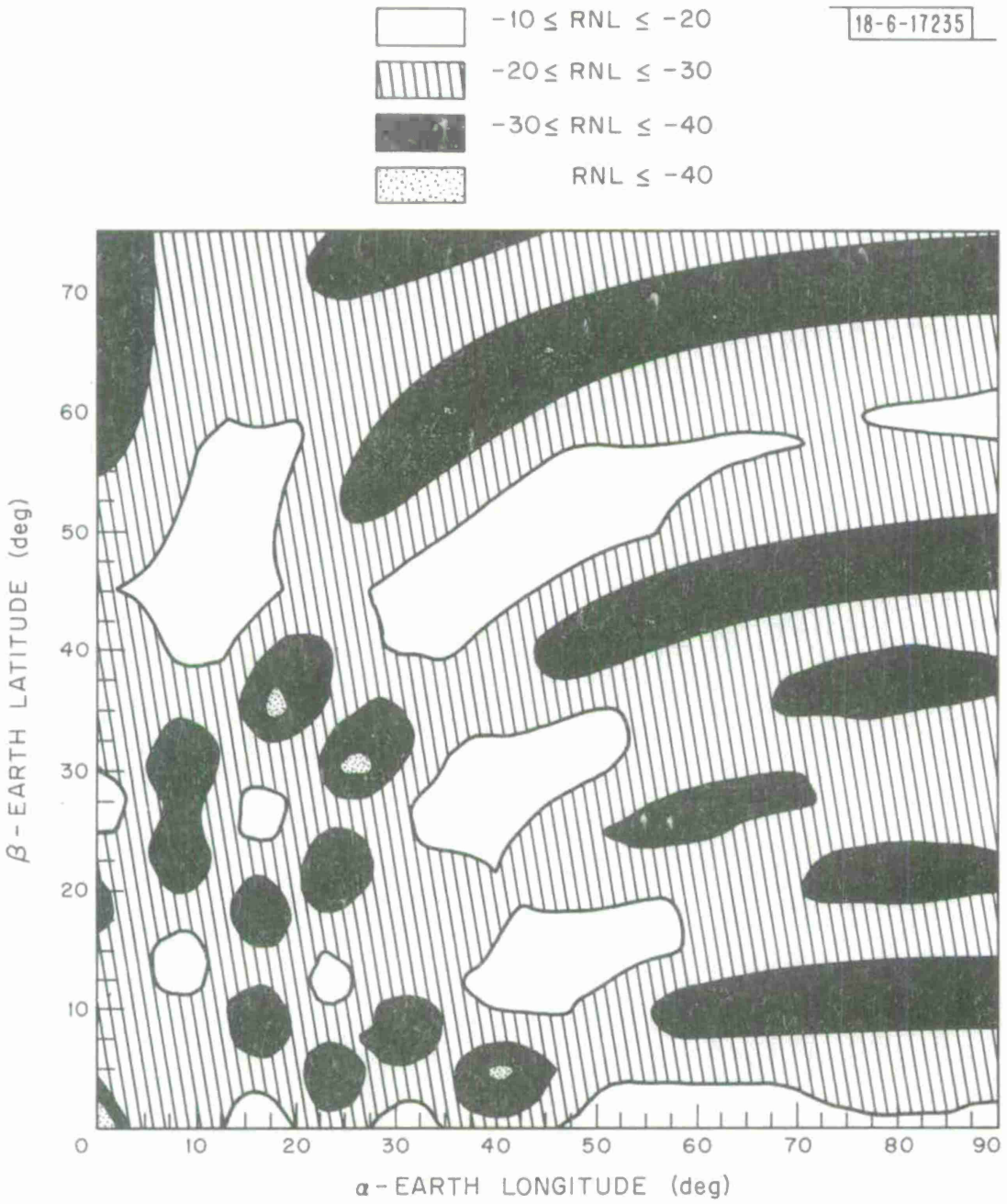

Fig. 13. Radiation pattern contour plot illustrating the null performance for the 61-element feed system at f = 8.15 GHz.

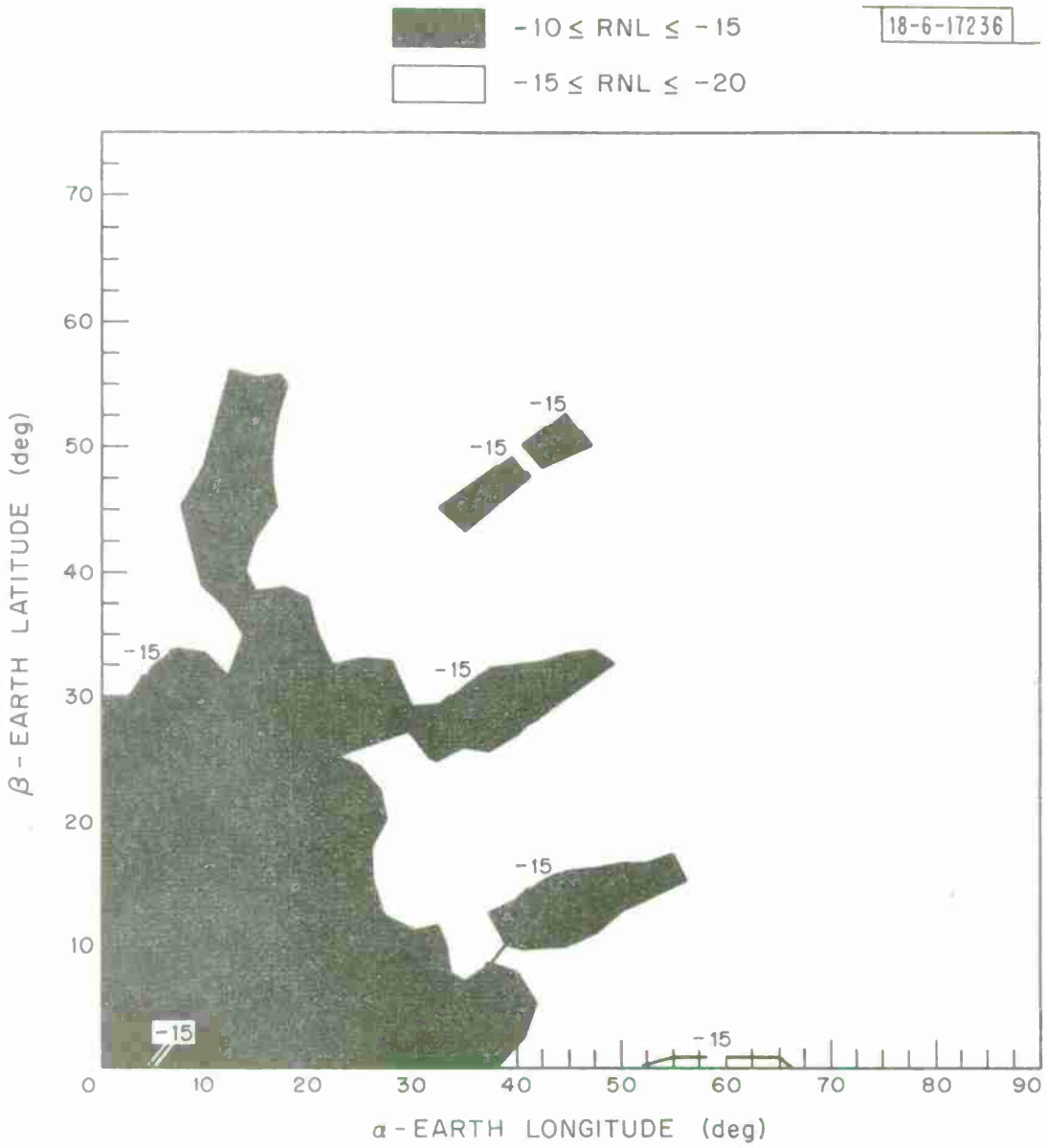

Fig. 14. Radiation pattern contour plot illustrating the null performance for the 61-element feed system at f = 8.325 GHz.

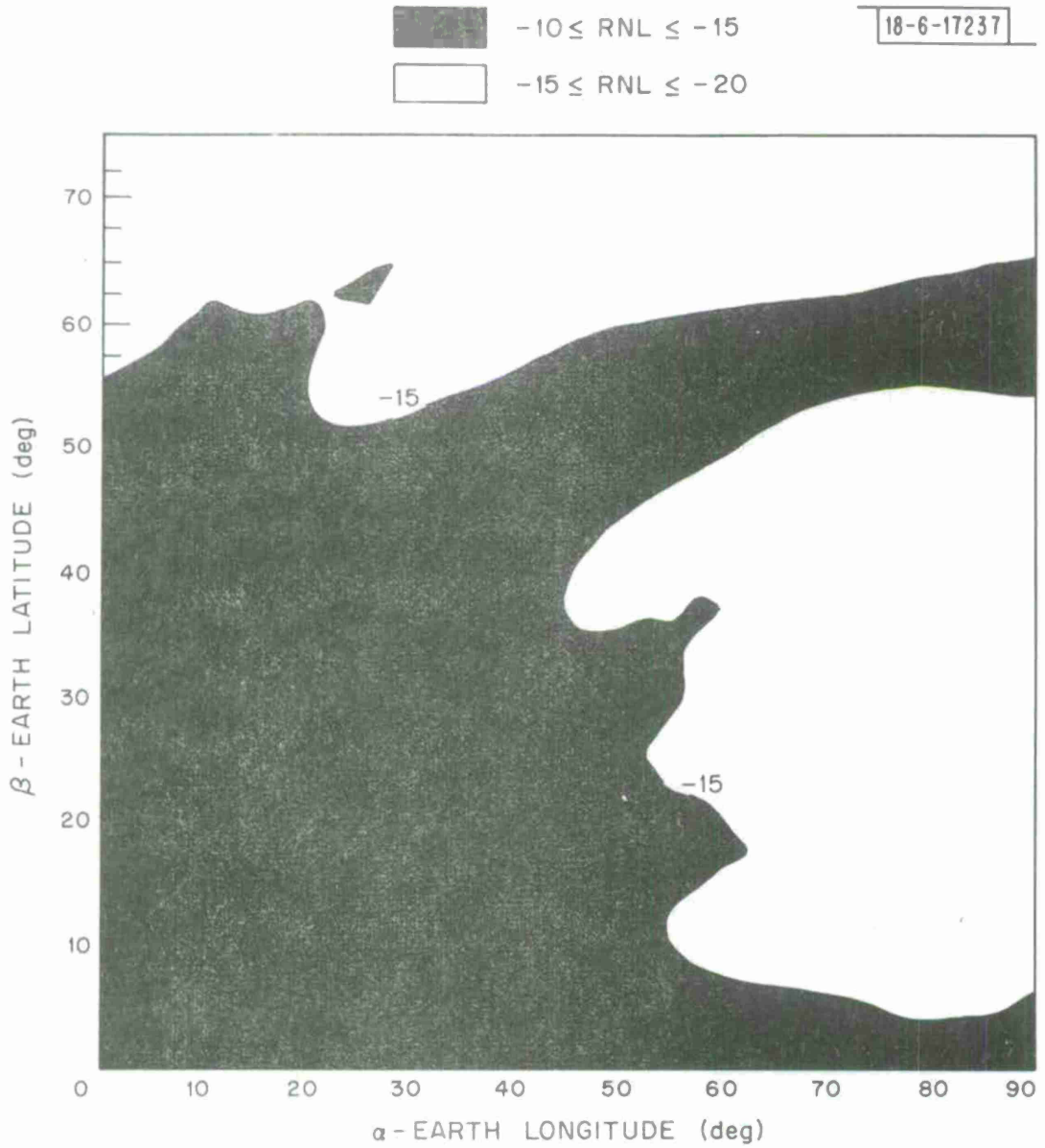

Fig. 15. Radiation pattern contour plot illustrating the null performance for the 61-element feed system at f = 7.975 GHz.

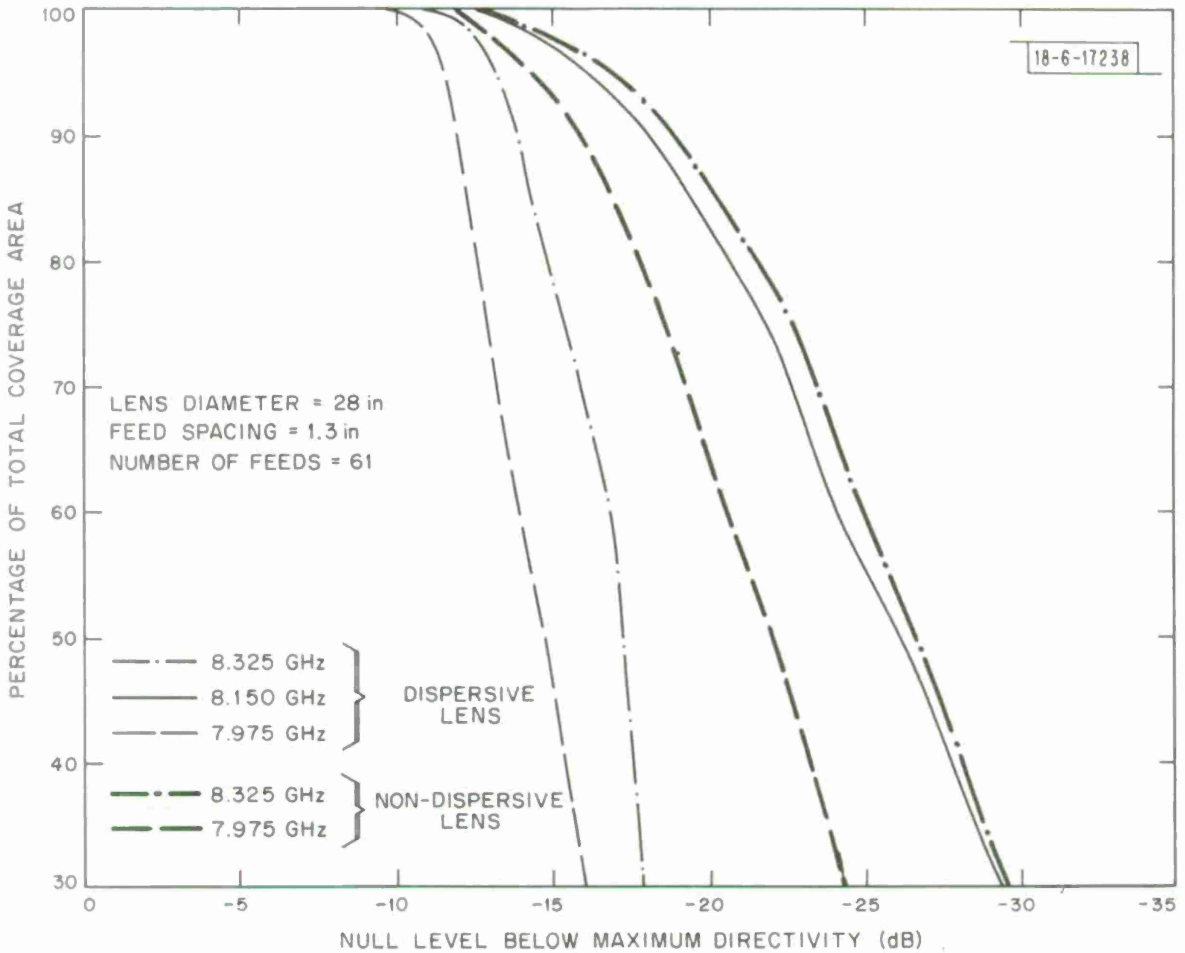

Fig. 16. Surface coverage area (in percent) vs. maximum null level for a 28-inch/61-feed MBA.

area the 61-element feed system has a somewhat poorer null level performance (3 dB) than the 19-beam system calculated on the basis of 65 ECPMIN patterns but significantly better nulling performance (by about 5 dB) than the 19-element system calculated on the basis of null steering and turning off a single beam. However, not shown explicitly in these figures is the fact that the null coverage area obtained with the 61-element feed system is considerably smaller than the null coverage area obtained with the 19-beam system which utilizes turning off two and three feeds to create a null.

Figure 16 also indicates the extent to which the jammer suppression can be improved if a nondispersive lens is used in lieu of a dispersive lens. It is interesting to observe that the null performance at 8.325 GHz for the nondispersive lens is slightly better than that obtained at 8.15 GHz. Also apparent from Fig. 16 (and Fig. 8) is the fact that the lens design frequency for optimizing the null coverage over the frequency band is not at the center of the receive band (8.15 GHz) but occurs at a slightly lower frequency. This is thought to be due to the fact that the insertion phase of the waveguide elements varies more rapidly at the lower frequencies, i.e., nearer to the waveguide cutoff frequency.

C. 61-Element Feed with 50-Inch Diameter Lens

Figures 17 and 18 illustrate the nulling performance for the 50-inch lens at the lens center frequency of 8.15 GHz. The data in these figures is calculated by considering a total of 1073 jammer locations on the earth between $0° \leq \alpha \leq 90°$ and $0° \leq \beta \leq 70°$ for $\Delta\alpha = \Delta\beta = 2.5°$. At each jammer location the best null level is determined from among the 165 possible ways of produc-

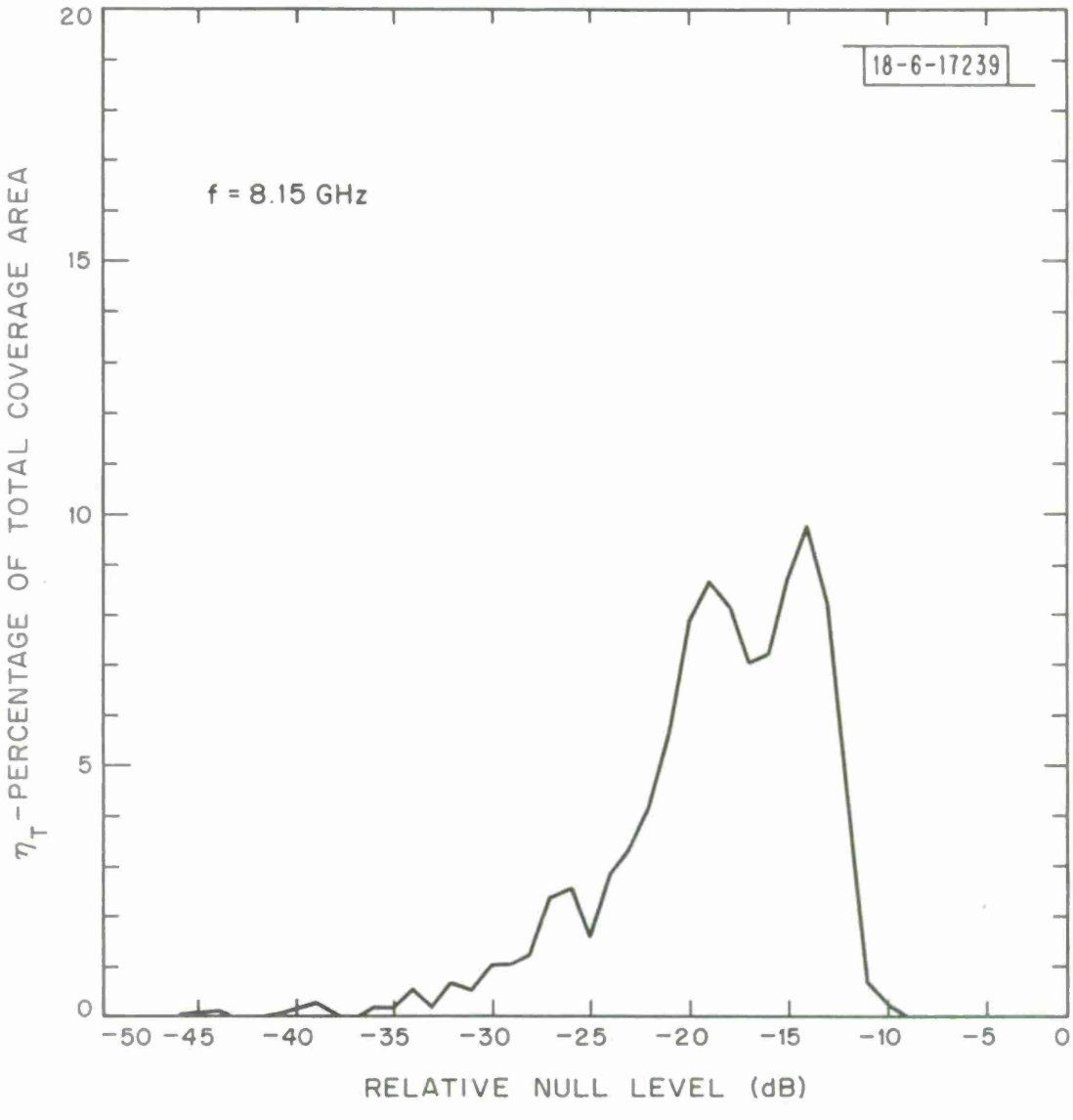

Fig. 17. Nulling performance for the 61-element feed cluster, 50-inch lens obtained by suppressing a single feed and null steering.

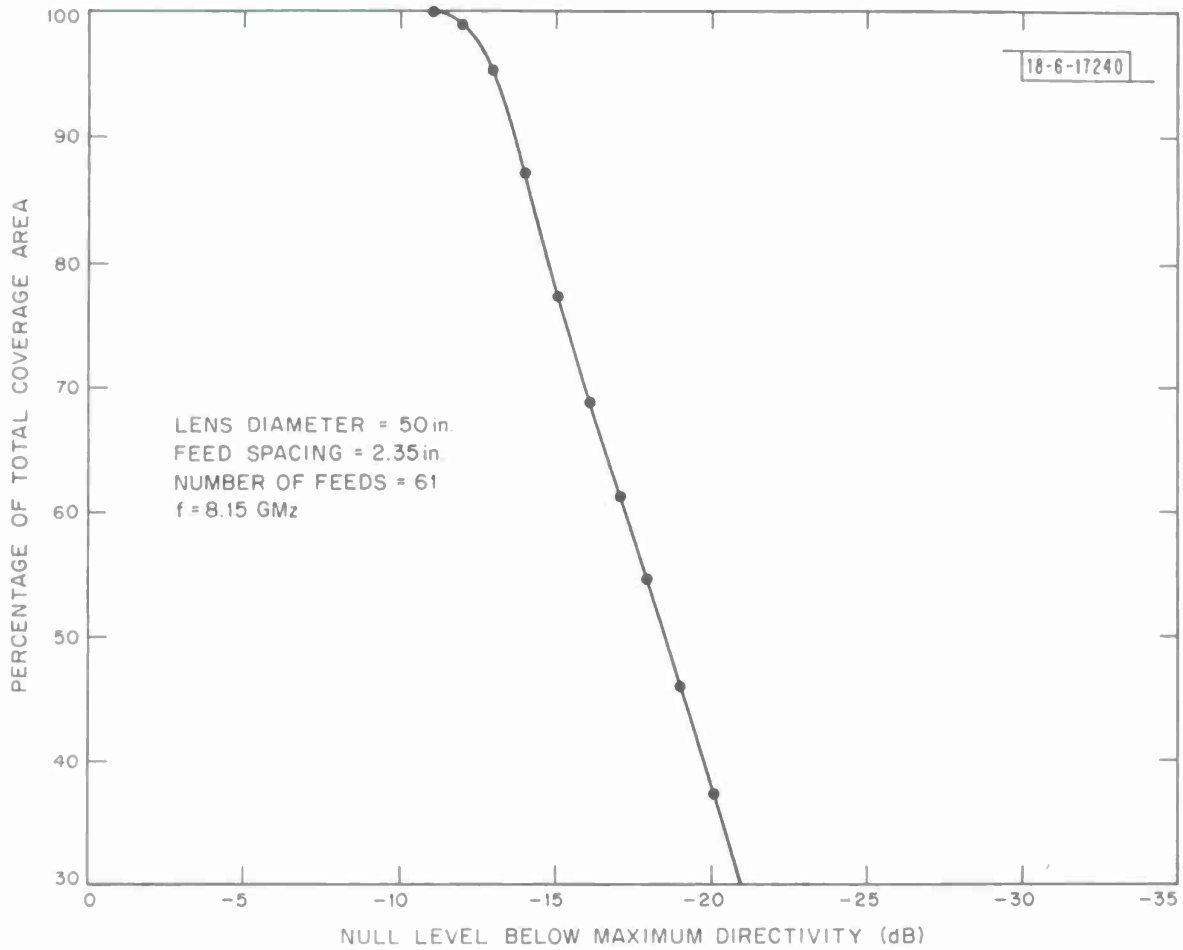

Fig. 18. Surface coverage area (in percent) vs. maximum null level for a 50-inch/61-feed MBA.

ing a null by suppressing a single beam and null steering (with n = 5). An interesting result of the calculations leading to Figs. 17 and 18 is the fact that approximately 98 percent of the 1073 jammer locations were suppressed using null steering. Less than 2 percent of the jammer locations were suppressed by turning off a single beam which clearly illustrates the superiority of null steering for producing deeper nulls.

From Fig. 18 it is apparent that the nulling performance of the 50-inch lens is degraded in comparison with the calculated results for the 28-inch lens using the 19-element feed (Fig. 8) and the 28-inch lens using the 61-element feed (Fig. 16). Based on the results of Fig. 18 it would appear that a more sophisticated nulling shceme is required in order to achieve acceptable AJ protection. However, it should be pointed out that the 50-inch diameter lens used in the calculations in Fig. 18 was obtained simply by scaling the dimensions of the 19-beam/28-inch lens by the ratio $\sqrt{3}$ (i.e., 50 inches $\simeq$ $\sqrt{3}$ x 28 inches). It may be possible to achieve a small improvement in the AJ performance by using a slightly different lens diameter.

IV. Radiation Pattern Calculations

A. Calculations for a 28-Inch Diameter Lens

In this section radiation pattern calculations are presented to illustrate the null coverage areas which can be achieved for various hypothetical jammers located over the surface of the earth. Figures 19 and 20 illustrate first the EC radiation contour plots for 19- and 61-element feed systems when all feed elements are excited. The contour plots are shown on a modified Orthographic projection for $-130° \leq \alpha \leq 50°$ and $-70° \leq \beta \leq 70°$, for a satellite located at $\alpha_o = -40°$. In order to represent the contour levels as power levels on the earth's surface it is necessary to include the power loss resulting from the difference in path length between the satellite and points located on the earth's surface. This power loss correction has been taken into account in plotting the contour levels in Fig. 19 and 20 as well as for the remaining contour plots to be presented in this section.

Consider now the situation in which a single, known jammer is located on the earth. For calculation purposes the jammer is assumed to be located at $\alpha = 37°$, $\beta = 55°$ with the satellite located at $\alpha_o = -40°$. Table III tabulates some possible ways of achieving a null at the jammer for the 19-element feed system with a single feed off (designated 19/1), two feeds off (19/2), three feeds off (19/3) and null steering (19/NS) and for the 61-element feed system with three feeds off (61/3). Associated with the five cases in Table III are the five contour plots in Figs. 21-25 which illustrate the null coverage areas obtained on the earth's surface. Clearly from Table III it is apparent that on the basis of jammer suppression the 19-element feed system

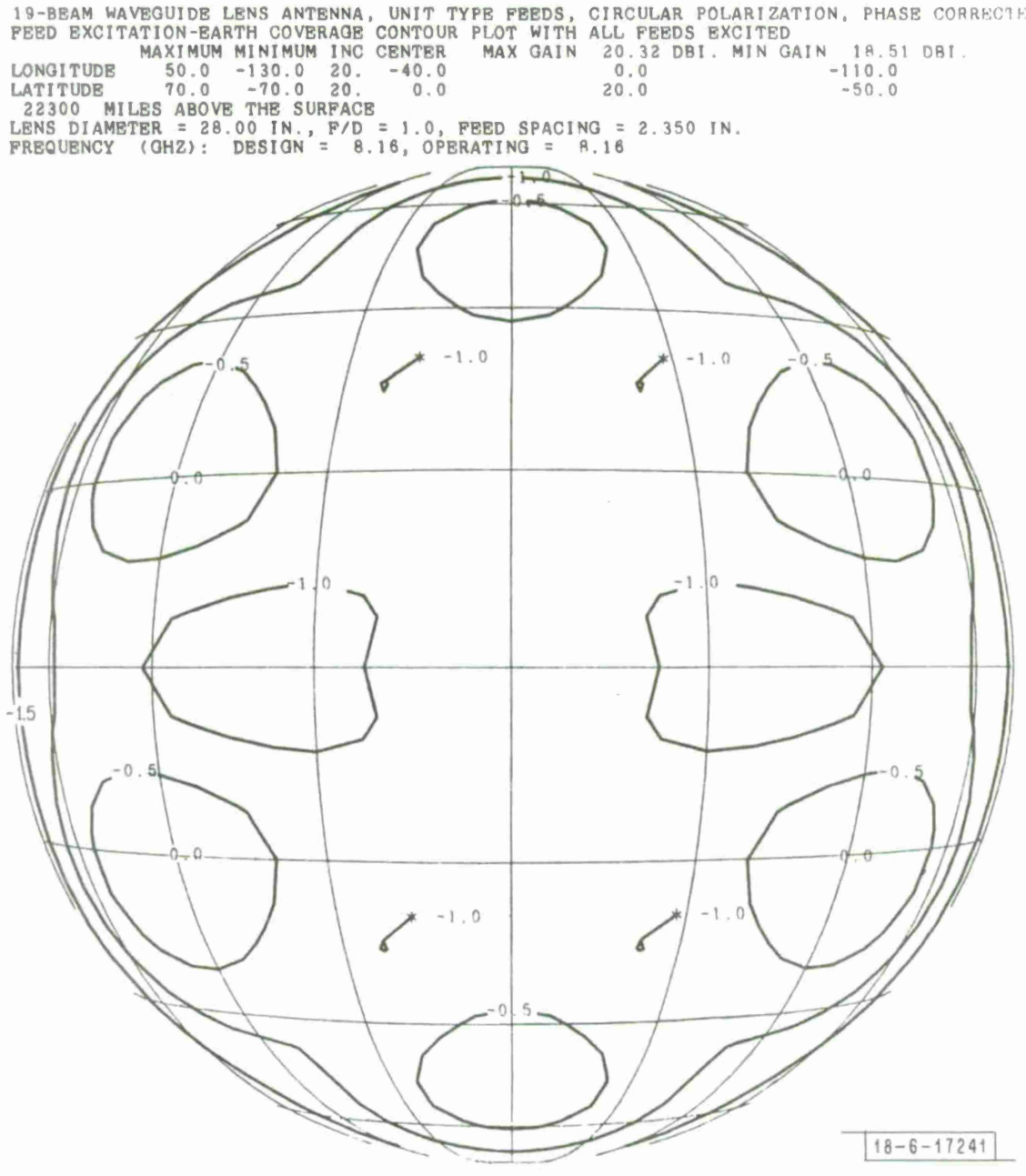

Fig. 19. Earth-coverage contour plot for the 28-inch lens with all 19 feeds excited.

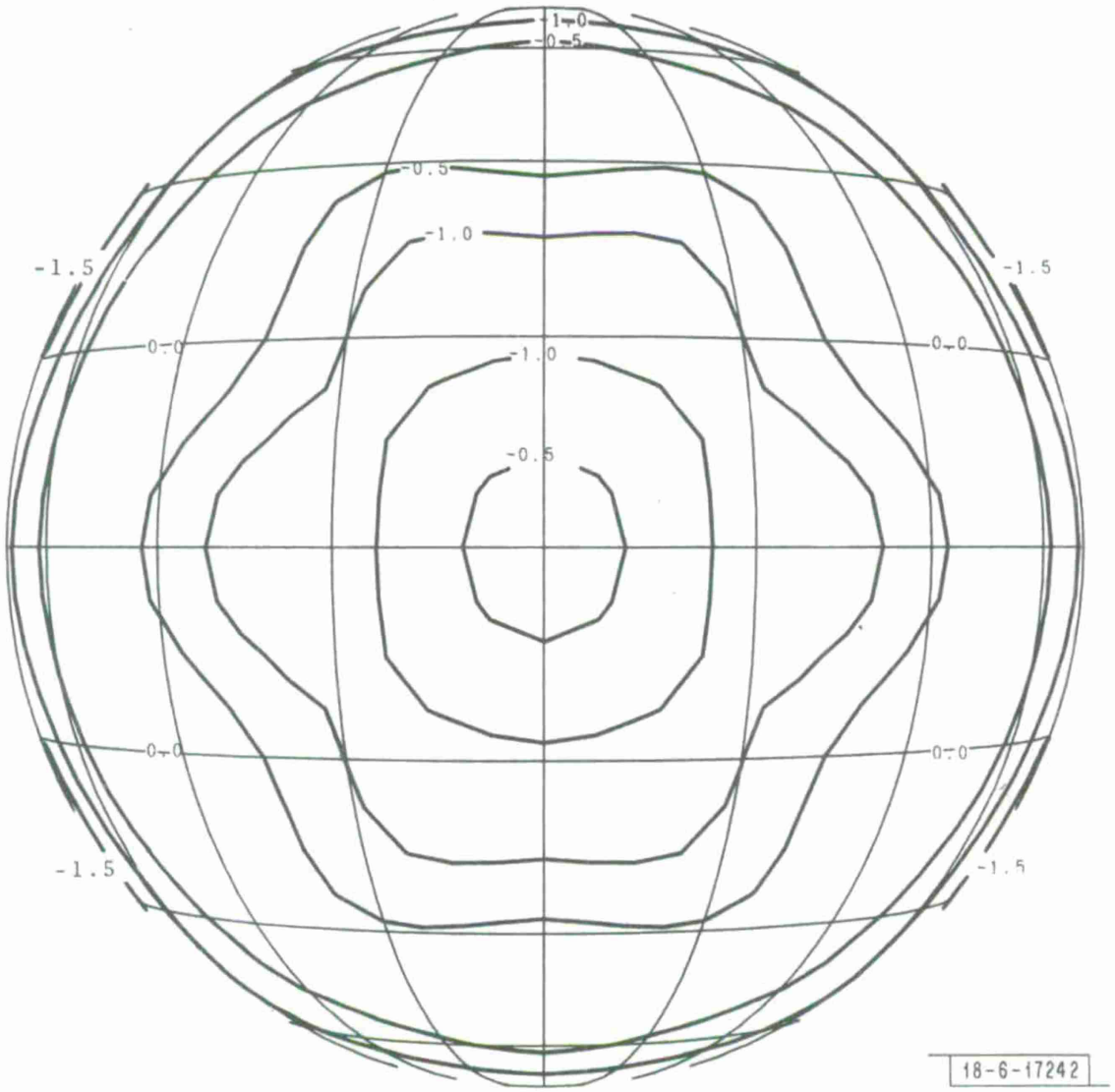

Fig. 20. Earth-coverage contour plot for the 28-inch lens with all 61 feeds excited.

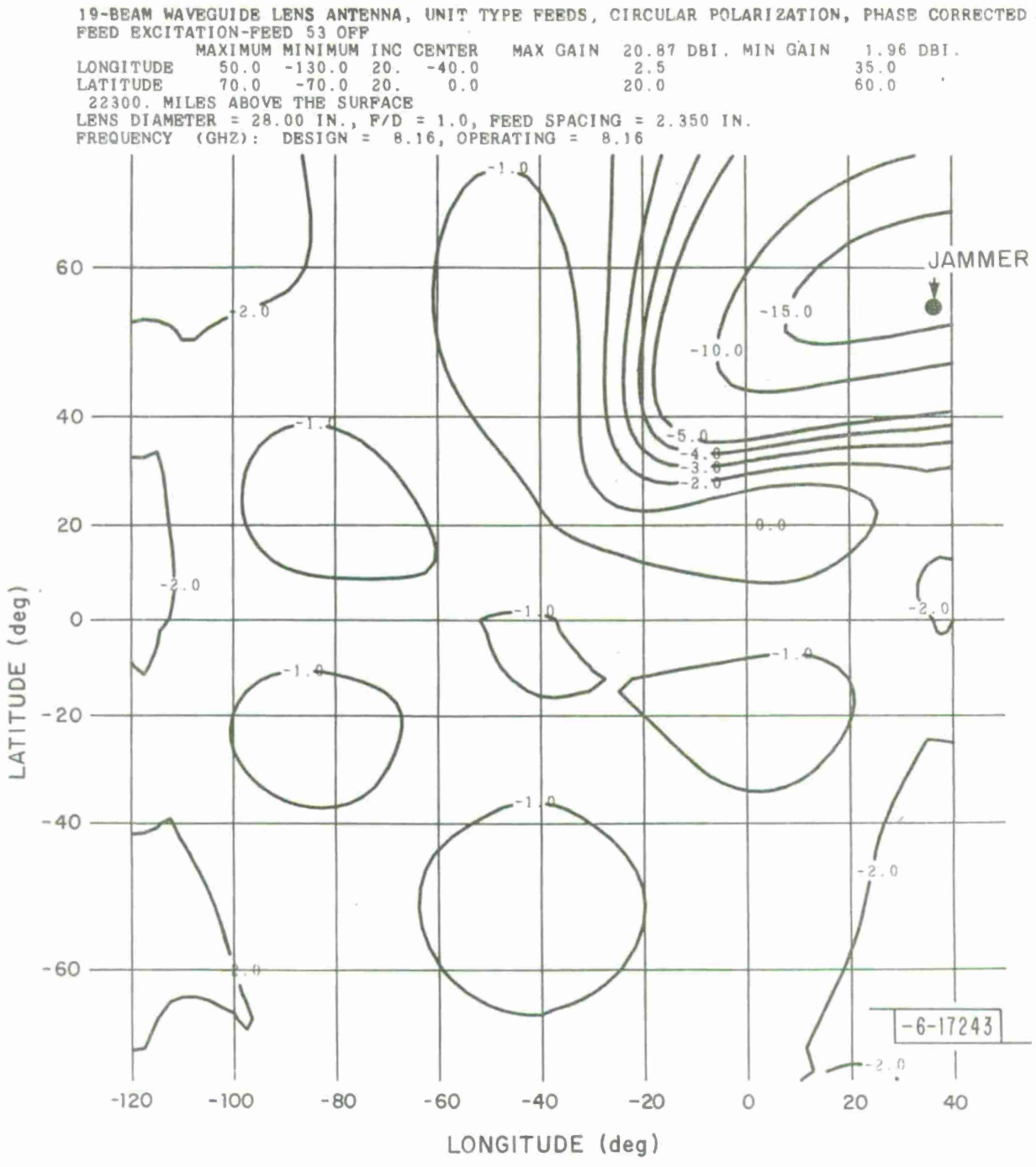

Fig. 21. Earth-coverage contour plot for the 28-inch lens with feed 53 off.

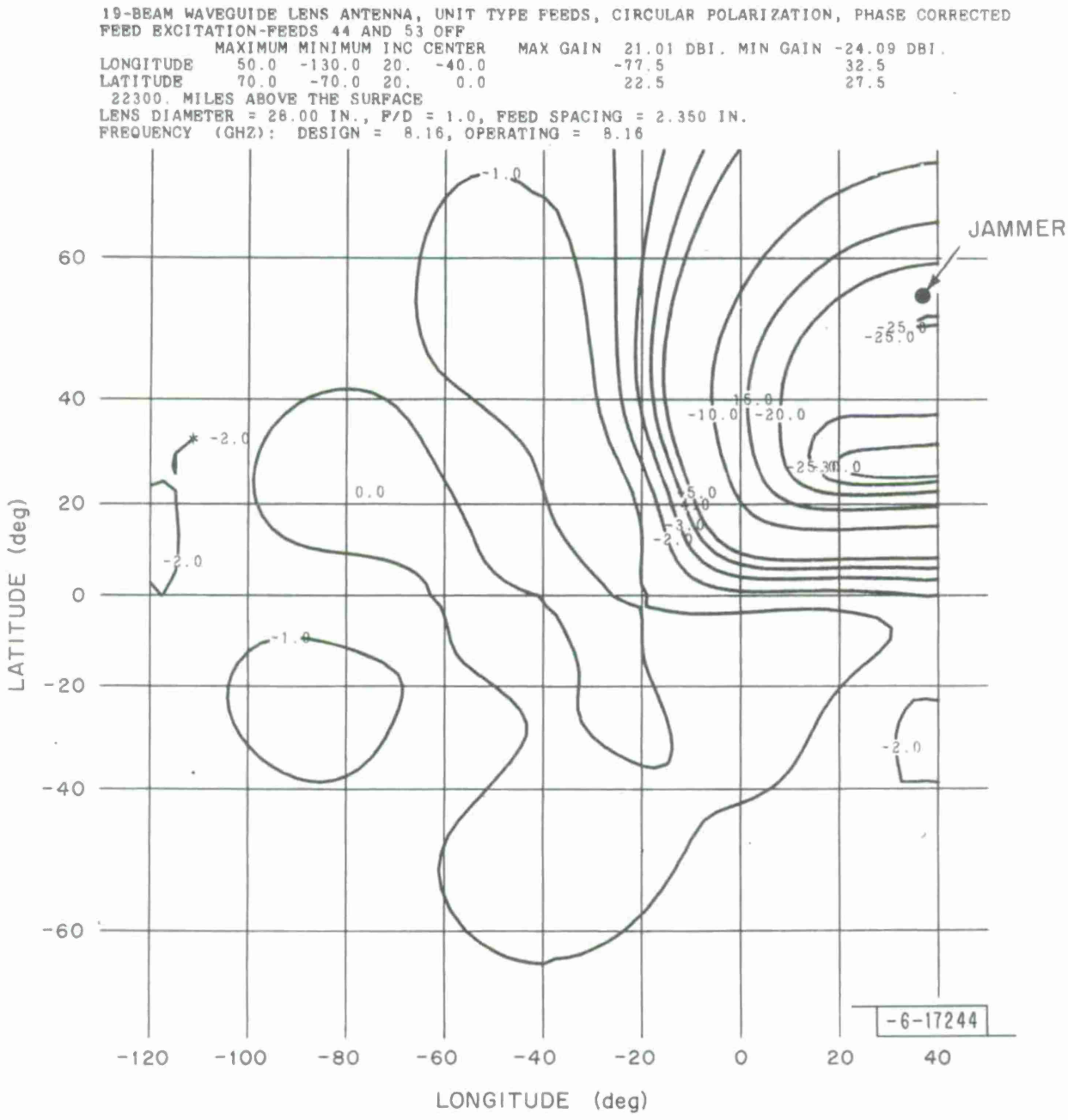

Fig. 22. Earth-coverage contour plot for the 28-inch lens with feeds 44 and 53 off.

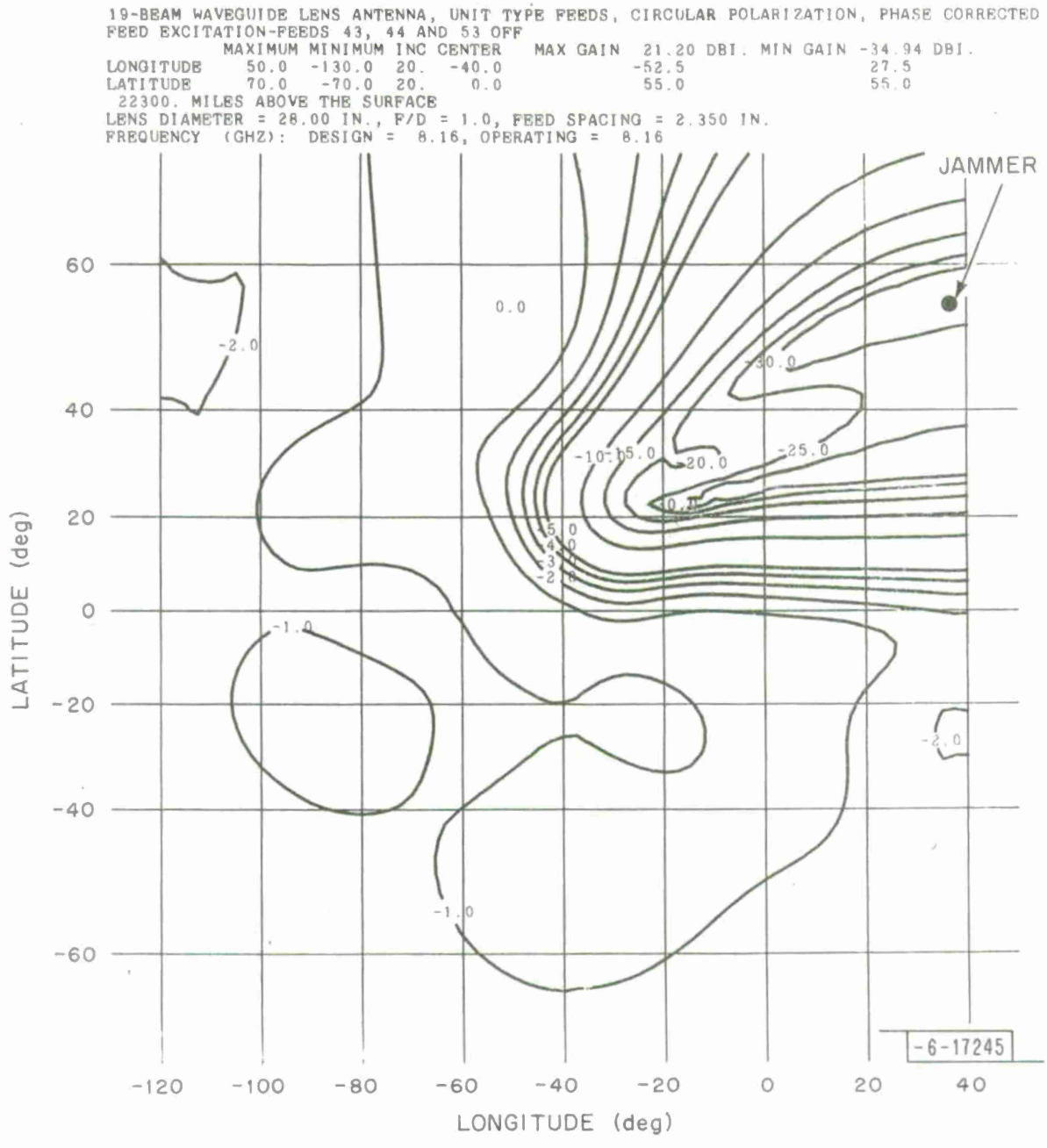

Fig. 23. Earth-coverage contour plot for the 28-inch lens with feeds 43, 44 and 53 off.

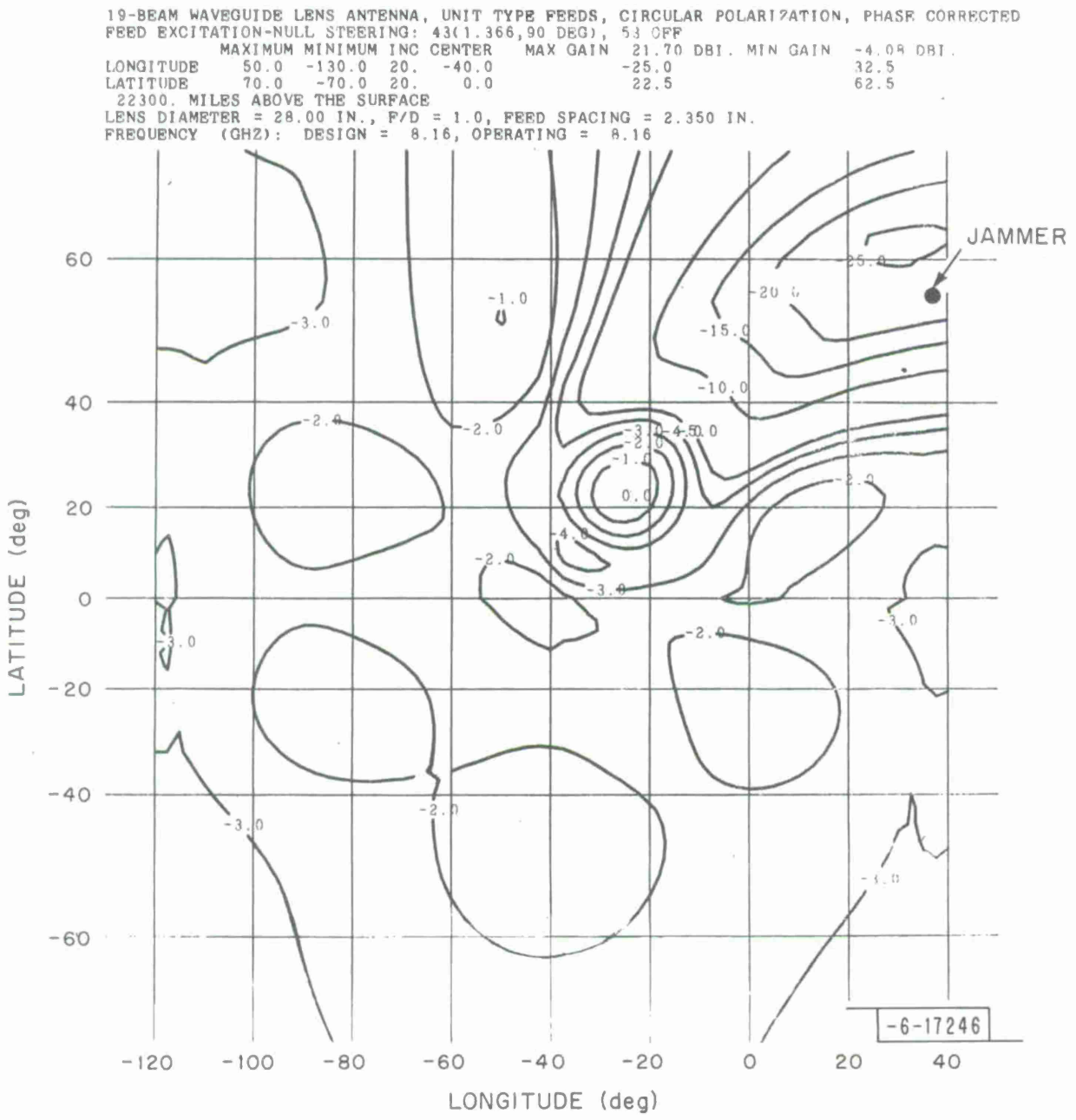

Fig. 24. Earth-coverage contour plot for the 28-inch lens obtained with null steering using feeds 43 and 53.

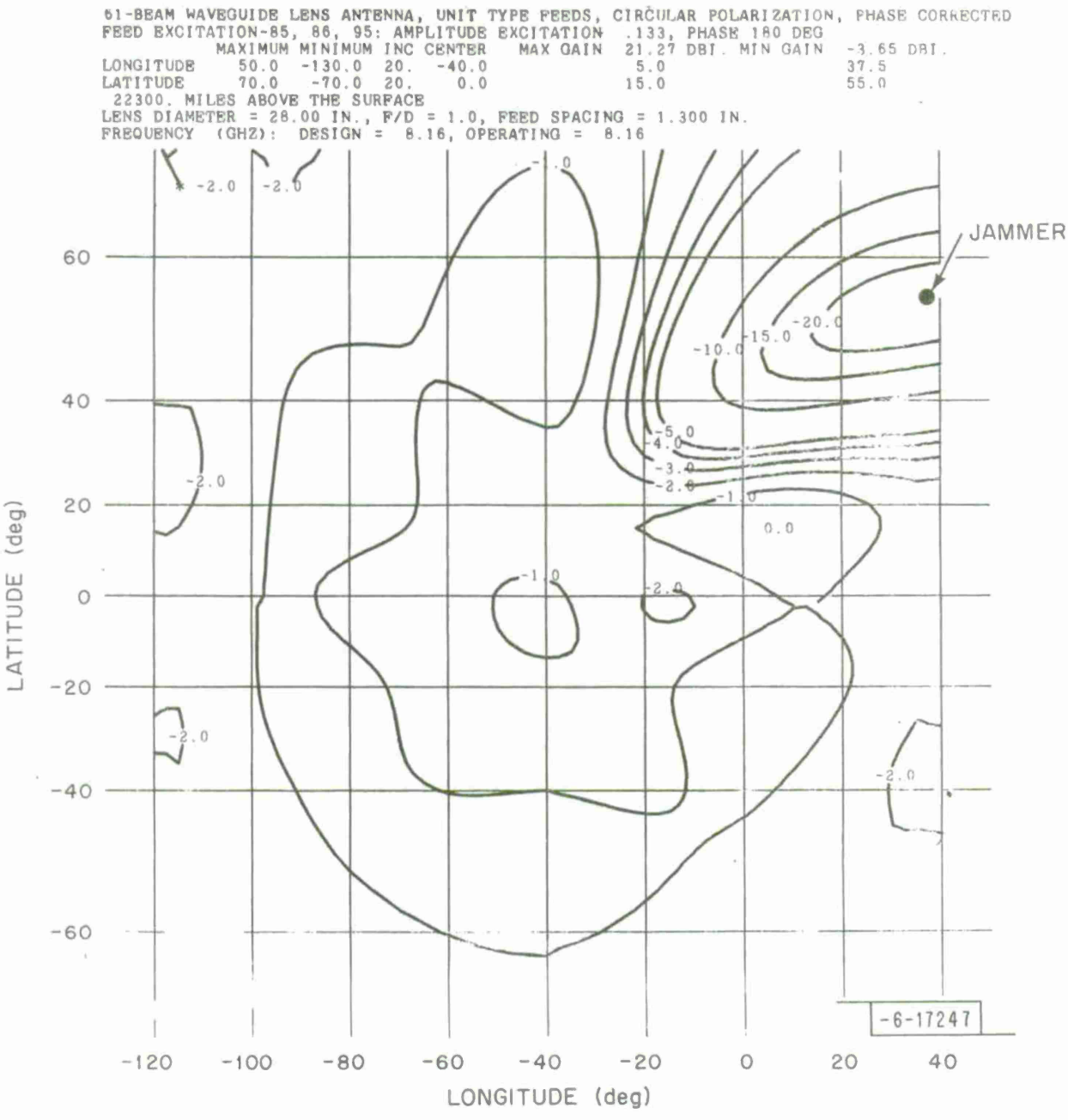

Fig. 25. Earth-coverage contour plot for the 28-inch lens/61-element cluster with feeds, 85, 86 and 95 excited 180° out-of-phase with relative power excitation of -17.52 dB.

with three feeds off is superior; however, its performance is compromised somewhat by the fact that the null coverage area is considerably larger than the other cases. In terms of null coverage areas, the surface area over which the directive gain is reduced 10 dB is more than four times larger for the 19/3 feed system than the null area produced by the 61/3 feed system.

TABLE III

Null Level Calculations at 8.15 GHz for a Single Jammer Located at $\alpha = 37°$, $\beta = 55°$ for a Satellite Location, $\alpha_o = -40°$

	Feed System	RNL (dB) at Jammer	Coverage Area x 10^6 (Statute Miles)^2 -10 dB	-20 dB	Feed Excitation
1.	19/1	-14.7	2.06	---	53 off
2.	19/2	-22.9	7.21	3.53	44, 53 off
3.	19/3	-38.1	11.38	6.60	44, 53, 43 off
4.	19/NS	-23.0	3.65	1.00	43 (1.366, 90°), 53 off
5.	61/3	-23.5	2.72	.52	85, 86, 95 with excitation .133, 180°

The large null coverage areas associated with the 28-inch lens can cause a serious degradation in the communications link depending upon where the jammer and desired users are located. In another case, for example, illustrated in Figs. 26 and 27 and tabulated in Table IV, for a jammer located at $\alpha = -82°$, $\beta = 23°$ communications over an area as large as several million square miles would certainly be degraded and possibly completely destroyed if the jammer were suppressed using the 19-beam system with two and three beams off. Even for the 19/1, 19/NS and 61/3-systems, the improvement is only

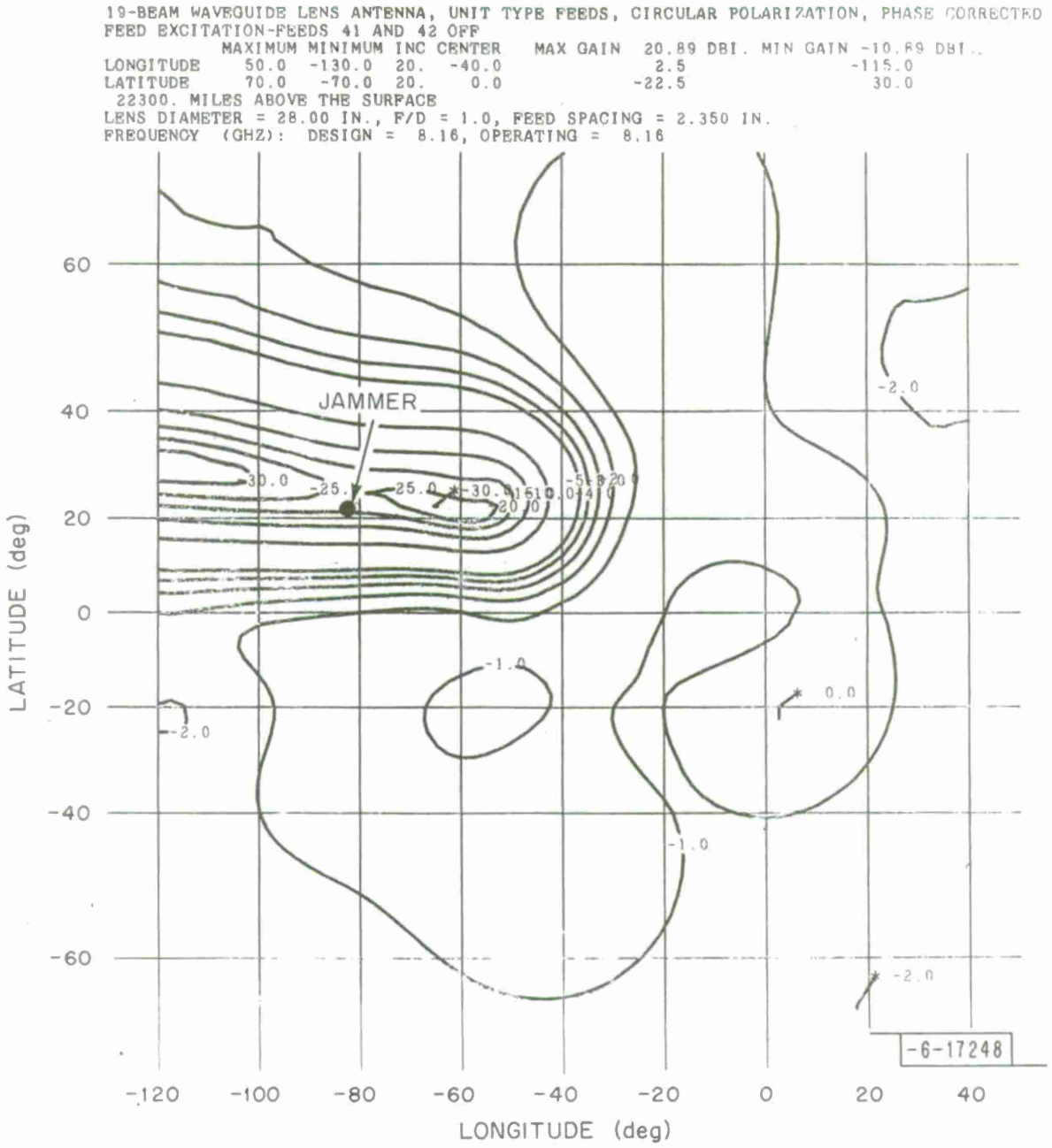

Fig. 26. Earth-coverage contour plot for the 28-inch lens with feeds 41 and 42 off.

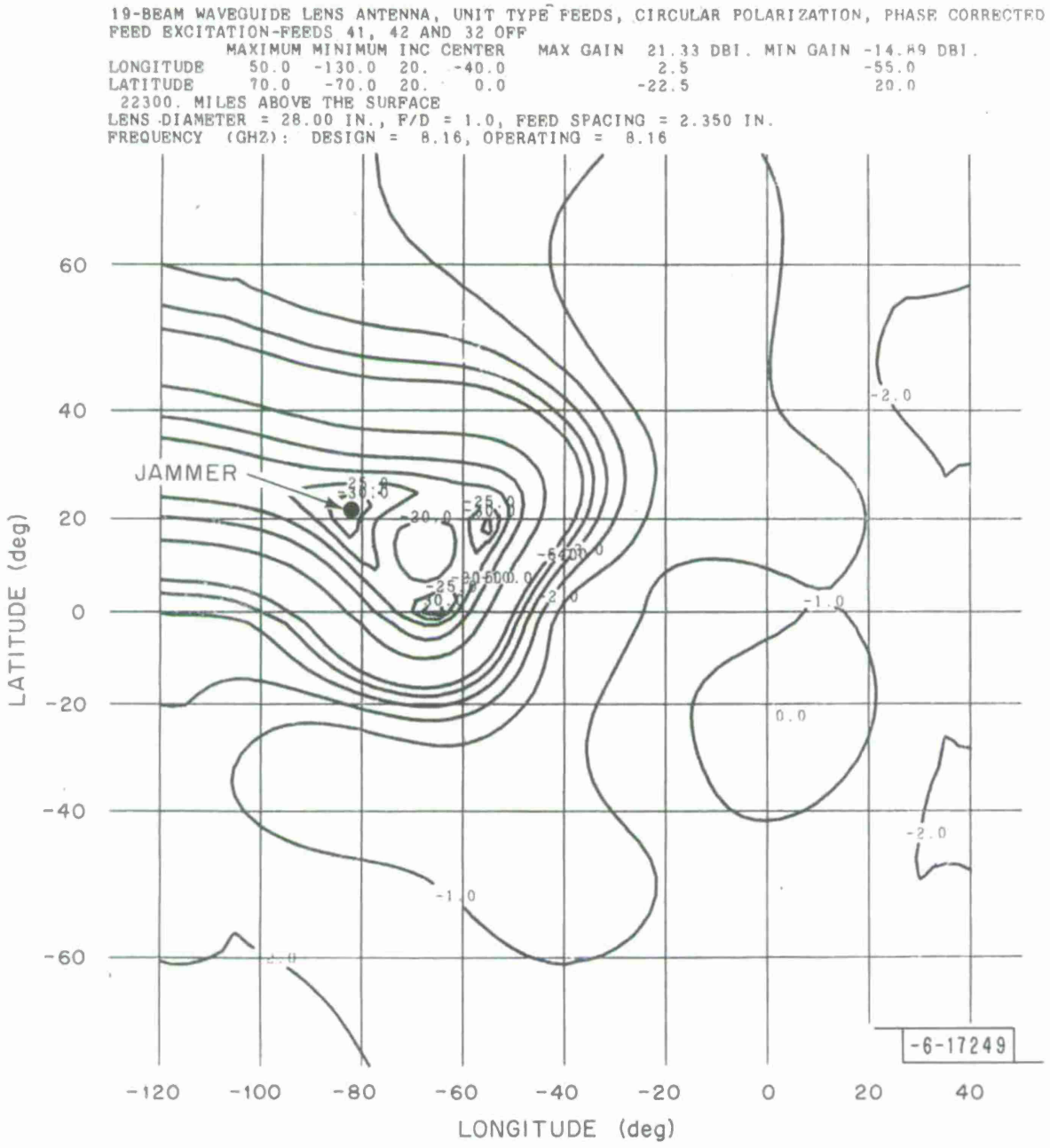

Fig. 27. Earth-coverage contour plot for the 28-inch lens with feeds 41, 42 and 32 off.

slightly better as indicated by the contour plots in Figs. 28-30.

TABLE IV

Null Level Calculations at 8.15 GHz for a Single Jammer Located at $\alpha = -82°$, $\beta = 23°$ for a Satellite Location, $\alpha_o = -40°$

	Feed System	RNL (dB) at Jammer	Coverage Area x 10^6 (Statute Miles)^2 -10 dB	-20 dB	Feed Excitation
1.	19/1	-12.4	3.95	1.66	41 off
2.	19/2	-22.6	7.67	3.20	41, 42 off
3.	19/3	-32.9	10.94	4.34	32, 41, 42 off
4.	19/NS	-19.1	3.03	.34	41 (.47, -90°), 42 (1.42, 90°)
5.	61/3	-29.2	5.03	2.48	62, 71, 72 with excitation .195, 180°

B. Calculations for a 50-Inch Diameter Lens

Figure 31 illustrates the EC contour pattern for a 50-inch lens plotted on a modified Orthographic projection. The agreement between this figure and the EC contour plots for the 28-inch lens (Figs. 19 and 20) is quite good; in all cases the maximum variation in power over the earth is approximately 1.5 dB.

The contour plots shown in Figs. 32 and 33 were calculated for the same jammer locations considered earlier (i.e., $\alpha = 37°$, $\beta = 55°$ and $\alpha = -82°$, $\beta = 23°$) and are representative of the type of null coverage areas which can be obtained with a 50-inch lens. In both figures jammer suppression is achieved by null steering and as shown in Table V, null levels of -17.7 dB and -15.0 dB were obtained. Although the calculated null levels at the jammer locations are somewhat larger for the 50-inch lens than those obtained with the

Fig. 28. Earth-coverage contour plot for the 28-inch lens with feed 41 off.

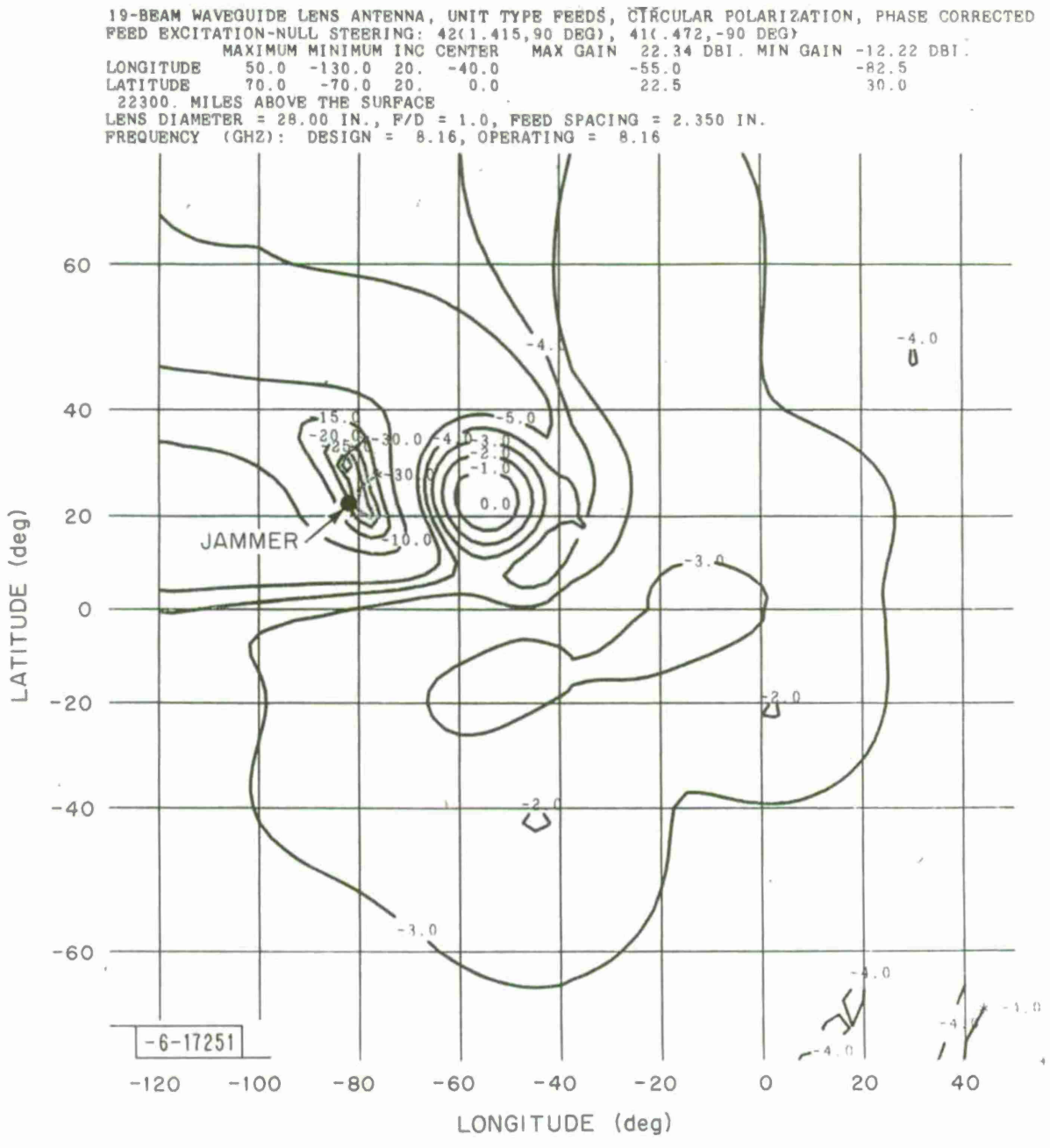

Fig. 29. Earth-coverage contour plot for the 28-inch lens obtained with null steering using feeds 41 and 42.

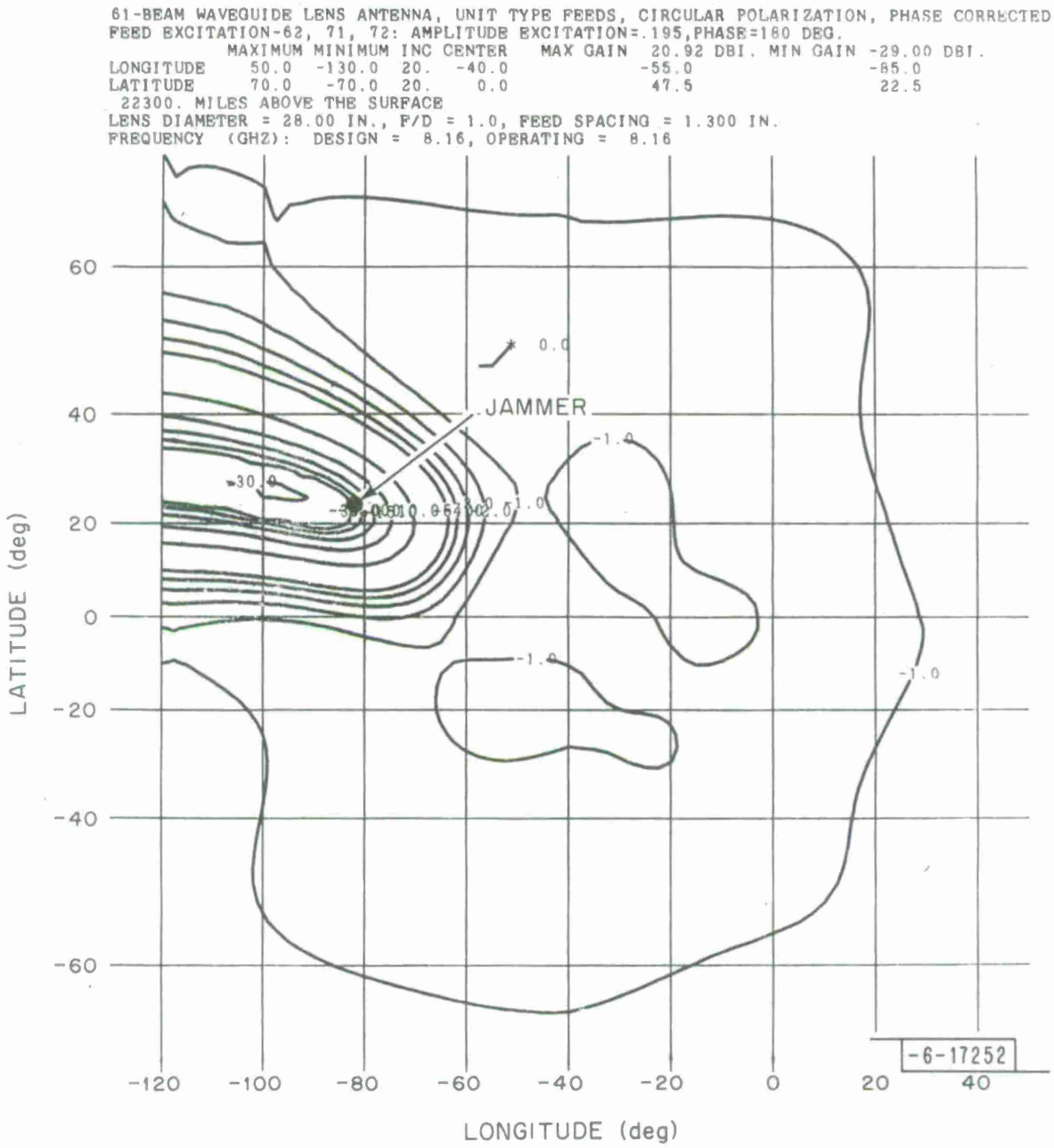

Fig. 30. Earth-coverage contour plot for the 28-inch lens/61-element cluster with feeds 62, 71 and 72 excited 180° out-of-phase with relative power excitation -14.2 dB.

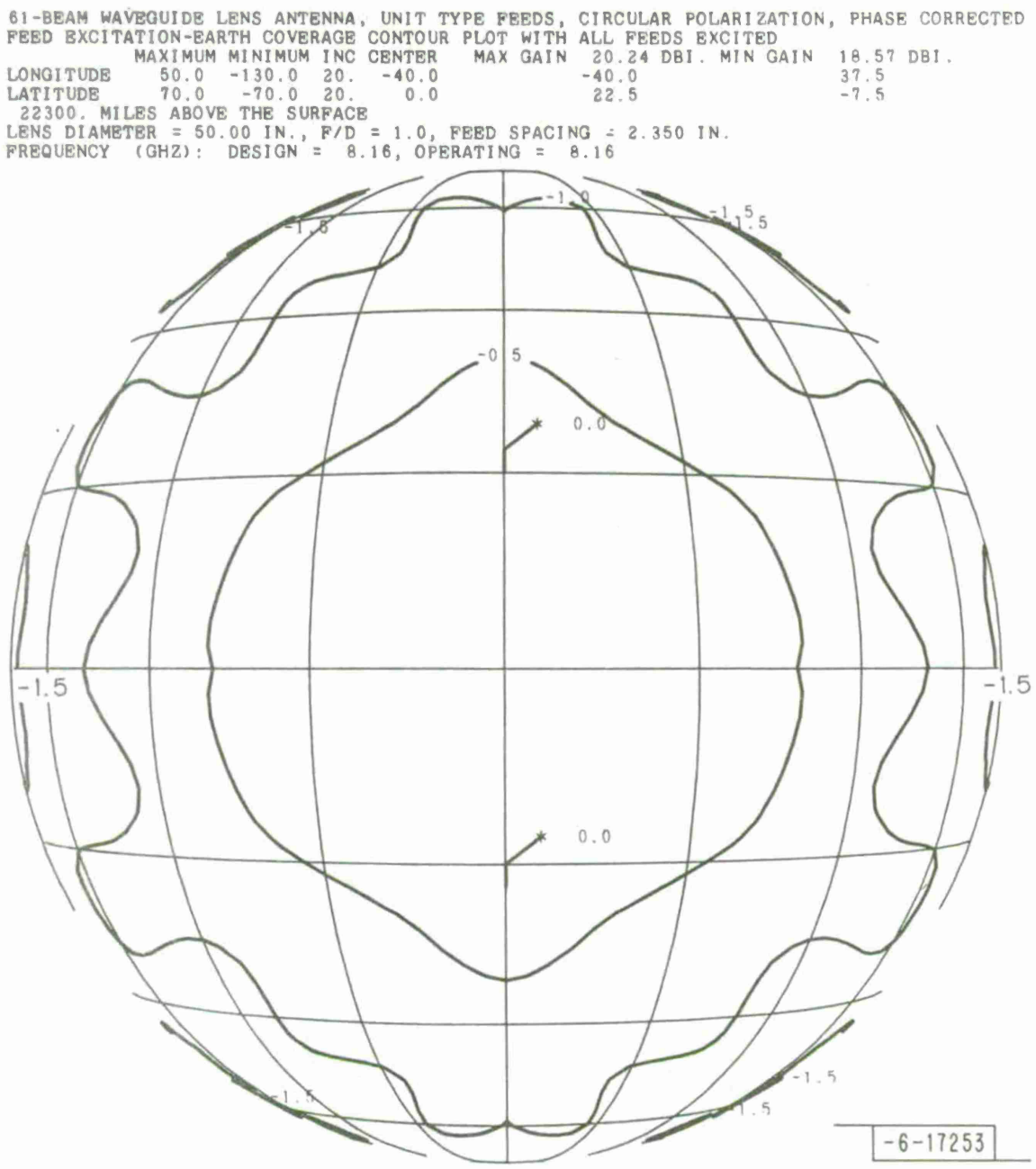

Fig. 31. Earth-coverage contour plot for the 50-inch lens with all 61 feeds excited.

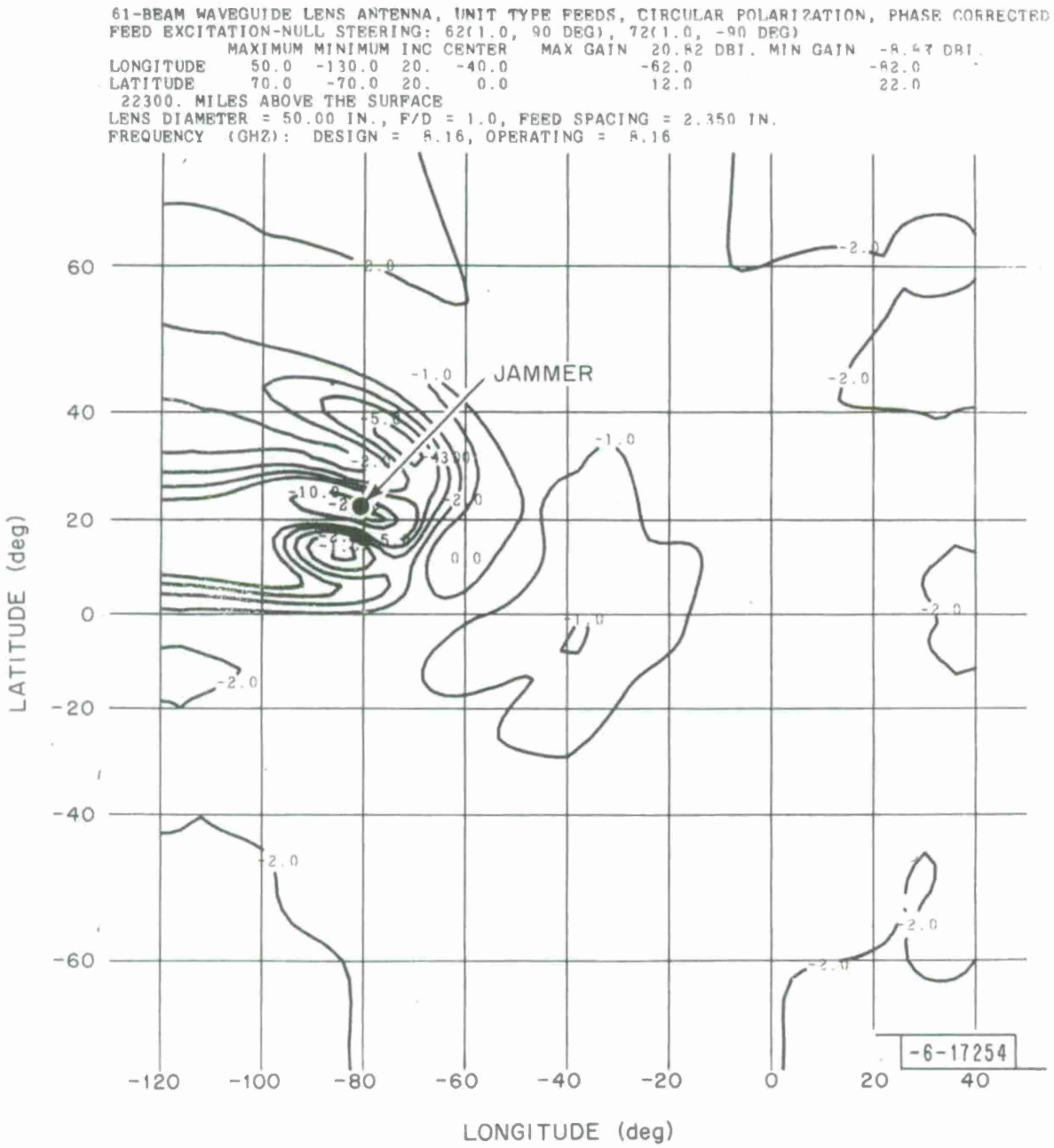

Fig. 32. Earth-coverage contour plot for the 50-inch lens obtained with null steering using feeds 62 and 72.

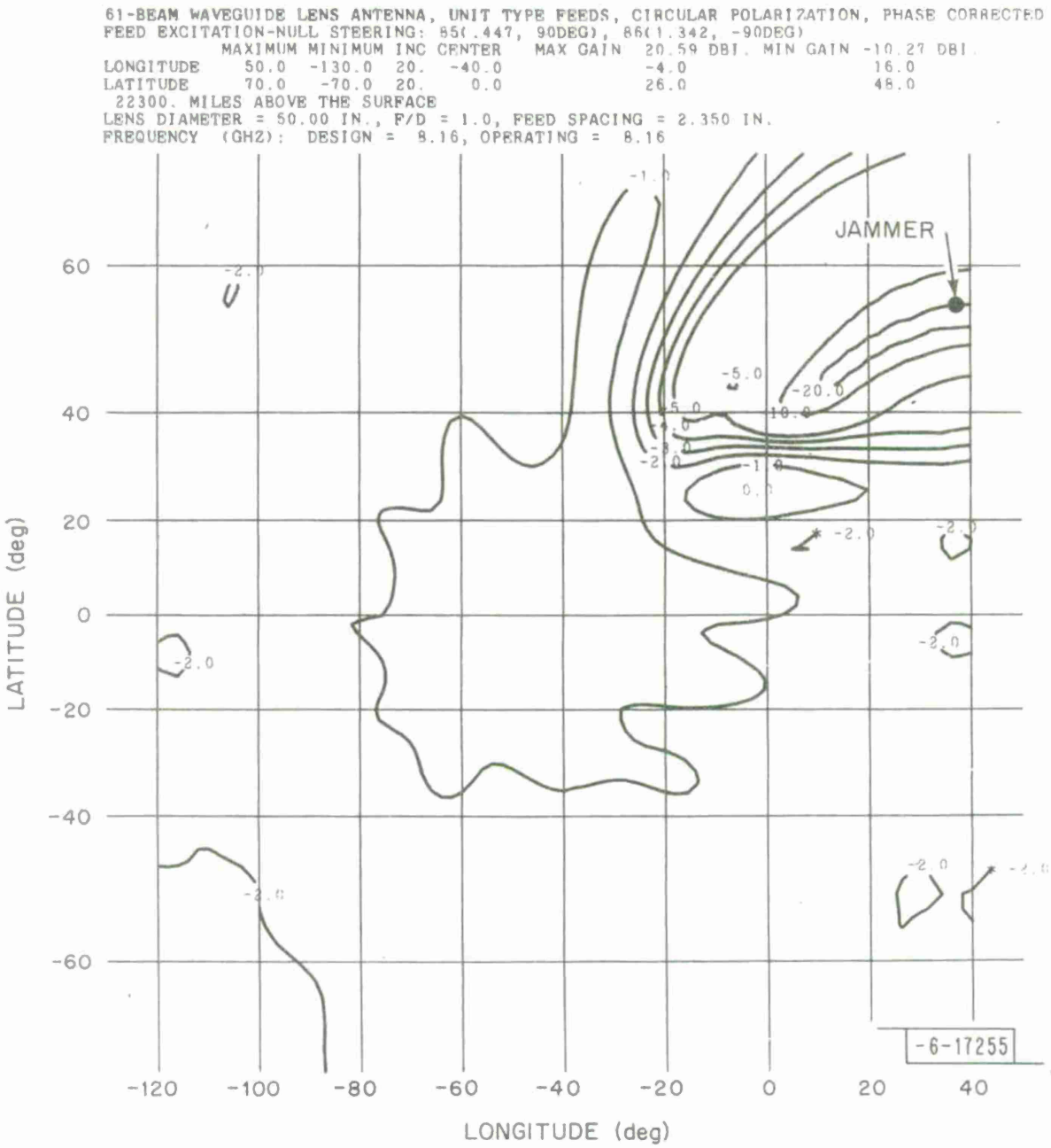

Fig. 33. Earth-coverage contour plot for the 50-inch lens obtained with null steering using feeds 85 and 86.

28-inch lens (see Tables III and IV) using null steering, the reduction in null coverage area which can be achieved with the 50-inch lens is quite significant. Considering the -10 dB coverage area as an example, the 50-inch lens produces a null coverage area of 319,000 square miles for the jammer located at $\alpha = -82°$, $\beta = 23°$ which compares with a minimum coverage area of 3,030,000 square miles for the 19/NS, 28-inch lens.

TABLE V

Null Level Calculations at 8.15 GHz for a Single Jammer Located at (a) $\alpha = 37°$, $\beta = 55°$ and (b) $\alpha = -82°$, $\beta = 23°$ for a Satellite Location, $\alpha_o = -40°$

	Feed System	RNL (dB) at Jammer	Coverage Area x 10^6 (Statute Miles)^2 -10 dB	-20 dB	Feed Excitation
a.	61/NS	-17.7	.878	.208	85(.447, 90°), 86(1.324, -90°)
b.	61/NS	-15.0	.319	.035	62(1, 90°), 72(1, -90°)

V. Conclusions

In this note calculations were presented describing the jamming suppression obtained with three different multiple-beam antennas: (1 and 2) a 28-inch diameter lens with 19- and 61-element feeds and (3) a 50-inch lens with a 61-element feed cluster. In all three cases, the jammer discrimination was obtained on the basis of shaping the radiation pattern by varying the amplitude excitation of the feed cluster.

Of the three MBA's, those using the 28-inch lens were found to produce the best performance on the basis of achieving the lowest null level at the jammer, however, the excessively large null coverage areas obtained with this lens severely limits its usefulness as a practical system. For the larger 50-inch lens, it was found that a jammer suppression of approximately 18 dB could be achieved over 50 percent of the coverage area using null steering and single beam suppression. To achieve levels significantly lower than this would require either (1) compromising the null coverage area by turning off more than one feed or (although less harmful in 50" than in 28") (2) utilizing a more sophisticated scheme of amplitude and phase control over the feed excitation.

The AJ performance was found to be highly frequency dependent due to the dispersive properties of the waveguide lens media. Over the receive band of the DSCS III satellite, the null level can be expected to increase by several dB over the value obtained at the lens design frequency.

The methods used to produce nulls were deliberately restricted to control of amplitude, plus the switching of phase between very restricted states, in order to assess the performance of a relatively simple, non-

adaptive approach. It is to be expected that better performance than that reported here could be achieved, with the penalty of greater complexity, by a system incorporating phase variation and control of amplitude and phase by an adaptive feedback loop.

Acknowledgments

The author would like to extend his appreciation to T. M. Turbett for his assistance in writing the computer programs and to Dr. A. J. Simmons for his many helpful discussions and comments.

References

1. L. J. Ricardi, et al., "Some Characteristics of a Communication Satellite Multiple-Beam Antenna," Technical Note 1975-3, Lincoln Laboratory, M.I.T. (28 January 1975). DDC AD-A00640515.

2. A. R. Dion, "Optimization of a Communication Satellite Multiple-Beam Antenna," Technical Note 1975-39, Lincoln Laboratory, M.I.T. (27 May 1975). DDC AD-A01310415.

OUTSIDE DISTRIBUTION LIST

Army

Lt. Colonel J. D. Thompson
ATTN: DAMO-TCS
Department of the Army
Washington, D.C. 20310

Mr. D. L. LaBanca
U.S. Army Satellite Communications Agency
ATTN: AMCPM-SC511
Building 209
Fort Monmouth, N. J. 07703

Headquarters
Department of the Army
ATTN: DAMA-CSC
Washington, D.C. 20310

Navy

Dr. R. Connley
Office of Chief of Naval Operations
ATTN: 094H
Department of the Navy
Washington, D.C. 20350

Captain S. B. Wilson
Office of Chief of Naval Operations
ATTN: 941P2
Department of the Navy
Washington, D.C. 20350

Mr. D. McClure
Office of Naval Telecommunications System Architect
3801 Nebraska Avenue
Washington, D.C. 20390

LCDR George Burman
Naval Electronics Systems Command Headquarters
ATTN: PME-106
Department of the Navy
Washington, D.C. 20350

Marine Corps

Major G. P. Criscuolo
ATTN: CE
Headquarters, U.S. Marine Corps
Washington, D.C. 20380

Air Force

Colonel M. J. Stephenelli
ATTN: RDSC
Headquarters, U. S. Air Force
Washington, D.C. 20330

Lt. Colonel J. C. Wright
ATTN: PRCXP
Headquarters, U.S. Air Force
Washington, D. C. 20330

JCS

Lt. Colonel J. S. Tuck
Organization Joint Chiefs of Staff
ATTN: J-6
Washington, D.C. 20301

Mr. S. L. Stauss
Organization Joint Chiefs of Staff
ATTN: J-3
Washington, D.C. 20301

NSA

Mr. George Jelen, Jr.
National Security Agency
ATTN: S-26
Ft. George G. Meade, Md. 20755

Mr. David Bitzer
National Security Agency
ATTN: R-12
Ft. George G. Meade, Md. 20755

TRI-TAC

Mr. Paul Forrest
TRI-TAC
Ft. Monmouth, N. J. 07703

DCA

Capt. Register or Capt. Lauber
SAMSO
P. O. Box 92960
Worldway Postal Center
Los Angeles, CA 90009
(20 copies)

C. Bredall
Aerospace Corp.
Bldg. 110, R. 1364
2400 El Segundo, Blvd.
El Segundo, CA 90045
(5 copies)

Dr. Frederick E. Bond, Code 800
Defense Communications Agency
8th Street and South Courthouse Road
Arlington, Virginia
(5 copies)

Mr. Troy Ellington
Defense Communications Eng. Center
1860 Wiehle Avenue
R-405
Reston, Virginia 22090
(2 copies)

C. Sletten
Air Force Cambridge Research Lab.
L. G. Hanscom Field
Bedford, MA 01730

REPORT DOCUMENTATION PAGE

READ INSTRUCTIONS BEFORE COMPLETING FORM

1. REPORT NUMBER: ESD-TR-75-299

2. GOVT ACCESSION NO.:

3. RECIPIENT'S CATALOG NUMBER:

4. TITLE *(and Subtitle)*: Radiation Pattern Calculations for a Waveguide Lens Multiple-Beam Antenna Operating in the AJ Mode

5. TYPE OF REPORT & PERIOD COVERED: Technical Note

6. PERFORMING ORG. REPORT NUMBER: Technical Note 1975-25

7. AUTHOR*(s)*: Potts, Bing M.

8. CONTRACT OR GRANT NUMBER*(s)*: F19628-76-C-0002

9. PERFORMING ORGANIZATION NAME AND ADDRESS:
Lincoln Laboratory, M.I.T.
P.O. Box 73
Lexington, MA 02173

10. PROGRAM ELEMENT, PROJECT, TASK AREA & WORK UNIT NUMBERS:

11. CONTROLLING OFFICE NAME AND ADDRESS:
Defense Communications Agency
8th Street & So. Courthouse Road
Arlington, VA 22204

12. REPORT DATE: 14 October 1975

13. NUMBER OF PAGES: 68

14. MONITORING AGENCY NAME & ADDRESS *(if different from Controlling Office)*:
Electronic Systems Division
Hanscom AFB
Bedford, MA 01731

15. SECURITY CLASS. *(of this report)*: Unclassified

15a. DECLASSIFICATION DOWNGRADING SCHEDULE:

16. DISTRIBUTION STATEMENT *(of this Report)*:
Approved for public release; distribution unlimited.

17. DISTRIBUTION STATEMENT *(of the abstract entered in Block 20, if different from Report)*:

18. SUPPLEMENTARY NOTES:
None

19. KEY WORDS *(Continue on reverse side if necessary and identify by block number)*:

multiple-beam antenna	waveguide lens	AJ performance
DSCS III satellites	jammer suppression	null steering

20. ABSTRACT *(Continue on reverse side if necessary and identify by block number)*:

The jammer suppression obtained with a multiple-beam antenna (MBA) by radiation pattern shaping is studied for applications with the DSCS III satellites. Results are presented for three separate MBA designs each consisting of an X-band waveguide lens excited by a multi-element feed cluster located in its focal plane.

To demonstrate the AJ performance of each MBA, calculations were carried out for a large number of jammer locations distributed over the surface of the earth. At each location, the jammer suppression is achieved by adjusting the amplitude excitation of the feed elements to create an earth-coverage radiation pattern with a minimum located in the direction of the jammer.

Results which characterize the AJ performance of each MBA in terms of the null level at the jammer, null coverage area and frequency dependence are presented.